塾大学病院予防医療センター[6]、滋賀医科大学消化器内科[7])

炎症性腸疾患における生物学的製剤治療の医療経済学的効果に関する研究 - 多施設共同研究プロトコールの提案

○藤谷幹浩[1]、堂腰達矢[1]、伊藤貴博[1]，稲場勇平[1]，上野伸展[1]、盛一健太郎[1]、田邊裕貴[1]，前本篤男[2、3]、蘆田知史[2、3]、田倉智之[4]、高後　裕[1]（旭川医科大学内科学講座　消化器・血液腫瘍制御内科学分野[1]、旭川医科大学消化管再生修復医学講座[2]、札幌東徳洲会病院 IBD センター[3]、大阪大学大学院医学系研究科 医療経済産業政策学[4])

p-B) 臨床プロジェクト

B-(1)　診療標準化コアプロジェクト

B-(1)-1　潰瘍性大腸炎・クローン病の診断基準および重症度基準の改変　(10:25～10:50)

総括　松井敏幸　福岡大学筑紫病院消化器内科

潰瘍性大腸炎の「軽症」の定義作成にむけて

○松井敏幸[1]、長堀正和[2]、平井郁仁[1]、井上　詠[3]、仲瀬裕志[4]、岡崎和一[5]、鈴木康夫[6]、渡辺　守[2]（福岡大学筑紫病院消化器内科[1]、東京医科歯科大学消化器内科[2]、慶應義塾大学医学部消化器内科[3]、京都大学医学部消化器内科[4]、関西医科大学内科学第三講座[5]、東邦大学医療センター佐倉病院内科[6])

クローン病における小腸病変の内視鏡診断基準にむけて

○松井敏幸、平井郁仁、久部高司、松嶋　祐（福岡大学筑紫病院消化器内科)

B-(1)-2　診療ガイドライン作成・改訂 (10:50～11:10)

総括　上野文昭　大船中央病院消化器肝臓病センター

Evidence-Based Clinical Practice Guidelines for Crohn's Disease, Integrated with Formal Consensus of Experts in Japan:欧米のクローン病診療ガイドラインとの類似点・相違点

○松岡克善[1]、上野文昭[2]、松井敏幸[3]、松本誉之[4]、渡辺　守[5]、日比紀文[1]（慶應義塾大学消化器内科[1]、大船中央病院[2]、福岡大学筑紫病院消化器内科[3]、兵庫医科大学下部消化管内科[4]、東京医科歯科大学消化器病態学)

炎症性腸疾患診療ガイドラインの改訂作業

○上野文昭[1]、渡邉聡明[2]、井上 詠[3]、国崎玲子[4]、小金井一隆[5]、小林清典[6]、小林健二[7]、猿田雅之[8]、仲瀬裕志[9]、長堀正和[10]、平井郁仁[11]、本谷　聡[12]、松井敏幸[11]（大船中央病院[1]、東京大学腫瘍外科[2]、慶應義塾大学予防医療センター[3]、横浜市立大学市民総合医療センターIBD センター[4]、横浜市立市民病院外科[5]、北里大学東病院消化器内科[6]、聖路加国際病院一般内科[7]、東京慈恵会医科大学消化器肝臓内科[8]、京都大学医学部消化器内科[9]、東京医科歯科大学消化器内科[10]、福岡大学筑紫病院消化器内科[11]、札幌厚生病院 IBD センター[12])

B-(1)-3　標準化を目指した治療指針の改訂 (11:10～11:40)

総括　中村志郎　兵庫医科大学内科下部消化管科

治療の標準化を目指した潰瘍性大腸炎治療指針の改訂

松本譽之[1]、○中村志郎[1]、杉田　昭[2]、余田　篤[3]、蘆田知史[4]、安藤　朗[5]、伊藤裕章[6]、押谷伸英[7]、金井隆典[8]、鈴木康夫[9]、長堀正和[10]、松井敏幸[11]、佐々木巌[12]、友政　剛[13]、田尻　仁[14]、福永　健[1]、樋田信幸[1]（兵庫医科大学内科学下部消化管科[1]、横浜市民病院外科[2]、大阪医科大学小児科[3]、札幌東徳洲会病院 IBD センター[4]、滋賀医科大学消化器内科[5]、錦秀会インフュージョンクリニック[6]、泉大津市立病院消化器内科[7]、慶応義塾大学消化器内科[8]、東邦大学佐倉病院消化器病センター[9]、東京医科歯科大学消化器内科[10]、福岡大学筑紫病院消化器内科[11]、みやぎ健康プラザ[12]、パルこどもクリニック[13]、大阪府立急性期・総合医療センター小児科[14])

治療の標準化を目指したクローン病治療指針の改訂

松本譽之[1]、○中村志郎[1]、杉田　昭[2]、余田　篤[3]、蘆田知史[4]、安藤　朗[5]、伊藤裕章[6]、押谷伸英[7]、金井隆典[8]、鈴木康夫[9]、長堀正和[10]、松井敏幸[11]、佐々木巌[12]、友政　剛[13]、田尻　仁[14]、福永　健[1]、樋田信幸[1]（兵庫医科大学内科学下部消化管科[1]、横浜市民病院外科[2]、大阪医科大学小児科[3]、札幌東徳洲会病院 IBD センター[4]、滋賀医科大学消化器内科[5]、錦秀会インフュージョンクリニック[6]、泉大津市立病院消化器内科[7]、慶応義塾大学消化器内科[8]、東邦大学佐倉病院消化器病センター[9]、東京医科歯科　大学消化器内科[10]、福岡大学筑紫病院消化器内科[11]、みやぎ健診

プラザ[12]、パルこどもクリニック[13]、大阪府立急性期・総合医療センター小児科[14])

潰瘍性大腸炎、クローン病外科治療指針の改訂

○杉田　昭[1]、亀岡信悟[2]、二見喜太郎[3]、根津理一郎[4]、藤井久男[5]、楠　正人[6]、舟山裕士[7]、渡邉聡明[8]、福島浩平[9]、板橋道朗[2]、池内浩基[10]、飯合恒夫[11]、佐々木巌[12]、松本誉之[13]（横浜市立市民病院外科[1]、東京女子医大第二外科[2]、福岡大学筑紫病院外科[3]、大阪労災病院外科[4]、奈良県立医科大学中央内視鏡超音波部[5]、三重大学消化管・小児外科学[6]、東北労災病院大腸肛門外科[7]、東京大学腫瘍外科[8]、東北大学分子病態外科[9]、兵庫医科大学下部消化管外科[10]、新潟大学消化器、一般外科[11]、みやぎ健診プラザ[12]、兵庫医科大学下部消化管科[13])

B-(2)　画期的な診断・治療の開発プロジェクト　ー診断面からー

B-(2)-1　新たなデバイスを用いたクローン病小腸病変の診断と治療（11:40～12:10）

総括　松本主之　九州大学大学院病態機能内科学

クローン病の小腸狭窄に対する内視鏡的拡張療法　ー多施設共同前向き試験の登録状況と中間解析ー

○平井郁仁[1]、松本主之[2]、松井敏幸[1]（福岡大学筑紫病院消化器内科[1]、九州大学病態機能内科学[2])

本邦クローン病におけるカプセル内視鏡所見の検討

○松本主之[1]、江崎幹宏[2]（九州大学病態機能内科学[1]、九州大学病院消化管内科[2])

クローン病小腸病変に対するバルーン小腸内視鏡とMREの比較試験：国内多施設共同試験

○渡辺憲治[1]、十河光栄[1]、山上博一[1]、竹内　健[2]、鈴木康夫[2]、矢野智則[3]、歌野健一[4]、山本博徳[3]、平井郁仁[5]、松井敏幸[5]、長沼　誠[6]、日比紀文[6]、大塚和朗[7]、渡辺　守[7]（大阪市立大学大学院医学研究科消化器内科学[1]、東邦大学医療センター佐倉病院内科[2]、自治医科大学消化器内科[3]、自治医科大学放射線科[4]、福岡大学筑紫病院消化器内科[5]、慶應義塾大学医学部消化器内科[6]、東京医科歯科大学消化器病態学[7])

＜昼食・幹事会＞　（12:10～13:00）

B-(2)-2　癌サーベイランス法の確立　（13:00～13:25）

総括　渡邉聡明　東京大学臓器病態外科学講座腫瘍外科学（味岡洋一）

潰瘍性大腸炎に対する癌サーベイランス法の確立

○渡邉聡明[1]、味岡洋一[2]、松本譽之[3]、武林　亨[4]、井上永介[5]、飯塚文瑛[6]、五十嵐正広[7]、岩男　泰[8]、大塚和朗[9]、工藤進英[9]、小林清典[10]、佐田美和[10]、田中信治[11]、友次直輝[12]、樋田信幸[3]、平田一郎[13]、松本主之[14]、渡辺憲治[15]、上野文昭[16]、渡辺　守[9]、日比紀文[17]（東京大学腫瘍外科[1]、新潟大学大学院医歯学総合研究科分子・診断病理学分野[2]、兵庫医科大学下部消化管科[3]、慶応義塾大学医学部衛生学公衆衛生学[4]、北里大学薬学部臨床統計[5]、東京女子医科大学消化器病センター[6]、癌研有明病院内科[7]、慶應義塾大学病院予防医療センター[8]、東京医科歯科大学消化器病態学[9]、北里大学東病院内科[10]、広島大学病院内視鏡診療科[11]、慶應義塾大学クリニカルリサーチセンター[12]、藤田保健衛生大学消化管内科[13]、九州大学大学院病態機能内科学[14]、大阪市立大学医学部消化器内科[15]、大船中央病院・消化器肝臓病センター[16]、慶應義塾大学医学部消化器内科[17])

クローン病に合併した大腸癌のsurveillance program確立の検討(痔瘻癌を含む)ー多施設共同研究によるpilot studyの中間報告（第2報）ー

○杉田　昭[1]、小金井一隆[1]、二見喜太郎[2]、舟山裕士[3]、池内浩基[4]、根津理一郎[5]、板橋道朗[6]、飯合恒夫[7]、水島恒和[8]、荒木俊光[9]、渡邉聡明[10]、福島浩平[11]、佐々木巌[12]（横浜市立市民病院外科[1]、福岡大学筑紫病院外科[2]、東北労災病院大腸肛門外科[3]、兵庫医科大学下部消化管外科[4]、大阪労災病院外科[5]、東京女子医科大学第2外科[6]、新潟大学消化器・一般外科[7]、大阪大学消化器外科[8]、三重大学消化管・小児外科学[9]、東京大学腫瘍外科[10]、東北大学分子病態外科[11]、みやぎ健診プラザ[12])

B-(3)　画期的な診断・治療の開発プロジェクト　ー治療面からー

B-(3)-3　外科治療の現状・工夫・予後(13:25～14:35)

総括　杉田　昭　横浜市立市民病院外科

外科治療の現状、工夫、予後-プロジェクト研究の現状と方針-

○杉田 昭[1]、亀岡信悟[2]、二見喜太郎[3]、根津理一郎[4]、藤井久男[5]、楠 正人[6]、舟山裕士[7]、渡邉聡明[8]、福島浩平[9]、板橋道朗[2]、池内浩基[10]、飯合恒夫[11]、佐々木巌[12]（横浜市立市民病院外科[1]、東京女子医科大学第2外科[2]、福岡大学筑紫病院外科[3]、大阪労災病院外科[4]、奈良県立医科大学中央内視鏡超音波部[5]、三重大学消化管・小児外科学[6]、東北労災病院大腸肛門外科[7]、東京大学腫瘍外科[8]、東北大学分子病態外科[9]、兵庫医科大学下部消化管外科[10]、新潟大学消化器・一般外科[11]、みやぎ健診プラザ[12]）

クローン病の術後療法に関する調査研究

○福島浩平[1]、羽根田祥[2]、渡辺和宏[2]、鈴木秀幸[2]、柴田　近[2]、舟山裕士[3]、杉田　昭[4]、二見喜太郎[5]、畠山勝義[6]、藤井久男[7]、池内浩基[8]、吉岡和彦[9]、亀岡信悟[10]、渡邉聡明[11]、楠　正人[12]、木内喜孝[13]、松本譽之[14]、鈴木康夫[15]、渡辺　守[16]（東北大学大学院消化管再建医工学・分子病態外科学分野[1]、東北大学大学院生体調節外科学分野[2]、東北労災病院大腸肛門外科[3]、横浜市立市民病院外科[4]、福岡大学筑紫病院外科[5]、新潟大学消化器・一般外科[6]、奈良県立医科大学中央内視鏡・超音波部[7]、兵庫医科大学外科[8]、関西医科大学付属枚方病院外科[9]、東京女子医科大学第二外科[10]、東京大学腫瘍外科[11]、三重大学消化管・小児外科学[12]、東北大学大学院消化器内科分野[13]、兵庫医科大学内科学下部消化管科[14]、東邦大学医療センター佐倉病院内科[15]、東京医科歯科大学大学院消化器病態学分野[16]）

クローン病肛門病変の重症度

○二見喜太郎、東大二郎、氷川裕二、石橋由紀子（福岡大学筑紫病院外科）

潰瘍性大腸炎術後の消化管出血

福島浩平[1]、羽根田祥[2]、渡辺和宏[2]、○鈴木秀幸[2]、柴田　近[2]、舟山裕士[3]、杉田　昭[4]、二見喜太郎[5]、畠山勝義[6]、藤井久男[7]、池内浩基[8]、吉岡和彦[9]、亀岡信悟[10]、渡邉聡明[11]、楠　正人[12]（東北大学大学院分子病態外科学分野・消化管再建医工学研究分野[1]、東北大学大学院生体調節外科学分野[2]、東北労災病院大腸肛門外科[3]、横浜市立市民病院外科[4]、福岡大学筑紫病院外科[5]、新潟大学消化器・一般外科[6]、奈良県立医科大学中央内視鏡・超音波部[7]、兵庫医科大学外科[8]、関西医科大学附属牧方病院外科[9]、東京女子医科大学第二外科[10]、東京大学腫瘍外科[11]、三重大学消化管・小児外科学[12]）

回腸嚢炎に関する調査研究　―「難治」の定義について―

○福島浩平[1]、羽根田祥[2]、渡辺和宏[2]、鈴木秀幸[2]、柴田　近[2]、舟山裕士[3]、杉田　昭[4]、二見喜太郎[5]、畠山勝義[6]、藤井久男[7]、池内浩基[8]、小金井一隆[4]、飯合恒夫[6]、東大二郎[5]、吉岡和彦[9]、亀岡信悟[10]、渡邉聡明[11]、楠　正人[12]（東北大学大学院分子病態外科学分野・消化管再建医工学研究分野[1]、東北大学大学院生体調節外科学分野[2]、東北労災病院大腸肛門外科[3]、横浜市立市民病院外科[4]、福岡大学筑紫病院外科[5]、新潟大学消化器・一般外科[6]、奈良県立医科大学中央内視鏡・超音波部[7]、兵庫医科大学外科[8]、関西医科大学附属牧方病院外科[9]、東京女子医科大学第二外科[10]、東京大学腫瘍外科[11]、三重大学消化管・小児外科学[12]）

就学期における潰瘍性大腸炎難治例に対する外科治療の適応について-小児科医の意見；日本小児 IBD 研究会メンバー施設を中心としたアンケート調査

藤井久男[1]、○中川　正[2]、小山文一[1]、杉田　昭[3]、飯合恒夫[4]、池内浩基[5]、亀岡信悟[6]、楠　正人[7]、根津理一郎[8]、福島浩平[9]、二見喜太郎[10]、舟山裕士[11]、吉岡和彦[12]、渡邉聡明[13]、渡邊昌彦[14]（奈良県立医科大学病院附属中央内視鏡・超音波部[1]、奈良県立医科大学消化器・総合外科[2]、横浜市立市民病院外科[3]、新潟大学医歯学総合病院消化器・一般外科[4]、兵庫医科大学炎症性腸疾患センター[5]、東京女子医科大学第二外科[6]、三重大学大学院消化管・小児外科学[7]、大阪労災病院外科[8]、東北大学大学院医学系研究科外科病態学生体調節外科学[9]、福岡大学筑紫病院外科[10]、東北労災病院外科・大腸肛門外科[11]、関西医科大学香里病院外科[12]、東京大学腫瘍外科[13]、北里大学医学部外科[14]）

高齢者潰瘍性大腸炎に対する手術の検討-手術適応、手術時期、手術術式、予後-

○杉田 昭[1]、亀岡信悟[2]、二見喜太郎[3]、根津理一郎[4]、藤井久男[5]、楠 正人[6]、舟山裕士[7]、渡邉聡明[8]、福島浩平[9]、

板橋道朗[2]、池内浩基[10]、飯合恒夫[11]、佐々木巌[12]（横浜市立市民病院外科[1]、東京女子医科大学第２外科[2]、福岡大学筑紫病院外科[3]、大阪労災病院外科[4]、奈良県立医科大学中央内視鏡超音波部[5]、三重大学消化管・小児外科学[6]、東北労災病院大腸肛門外科[7]、東京大学腫瘍外科[8]、東北大学分子病態外科[9]、兵庫医科大学下部消化管外科[10]、新潟大学消化器・一般外科[11]、みやぎ健診プラザ[12]）

B-(4)　診療に伴う合併症/副作用および特殊型への対策プロジェクト

B-(4)-1　潰瘍性大腸炎合併サイトメガロウイルス腸炎および血栓症（14:35～15:15）

総括　鈴木康夫　東邦大学医療センター佐倉病院内科

潰瘍性大腸炎に合併するサイトメガロウイルス(CMV)再活性化症例に対する前向き研究　進捗状況

鈴木康夫[1]、石黒　陽[2]、仲瀬裕志[3]、大宮美香[4]、平井郁仁[5]、池田圭祐[6]、山田哲弘[1]、松岡克善[7]、○長沼　誠[7]、福地　工[8]、渡辺　守[9]（東邦大学医療センター佐倉病院内科[1]、弘前大学光学医療診療部[2]、京都大学消化器内科[3]、関西医科大学香里病院消化器内科[4]、福岡大学筑紫病院消化器科[5]、福岡大学筑紫病院病理[6]、慶應義塾大学医学部消化器内科[7]、大阪済生会中津病院消化器内科[8]、東京医科歯科大学消化器病態学[9]）

PCR法による難治性潰瘍性大腸炎合併サイトメガロウイルス感染性腸炎の診断能の比較検討

鈴木康夫[1]、石黒　陽[2]、○仲瀬裕志[3]、大宮美香[4]、平井郁仁[5]、池田圭祐[6]、山田哲弘[1]、松岡克善[7]、長沼　誠[7]、福地　工[8]、渡辺　守[9]（東邦大学医療センター佐倉病院内科[1]、弘前大学光学医療診療部[2]、京都大学消化器内科[3]、関西医科大学香里病院消化器内科[4]、福岡大学筑紫病院消化器科[5]、福岡大学筑紫病院病理[6]、慶應義塾大学医学部消化器内科[7]、大阪済生会中津病院消化器内科[8]、東京医科歯科大学消化器病態学[9]）

潰瘍性大腸炎周術期の血栓塞栓症の予防に関する前向き研究

亀岡信悟[1]、板橋道朗[1]、小川真平[1]、○杉田　昭[2]、福島浩平[3]、渡邉聡明[4]、飯合恒夫[5]、池内浩基[6]、楠　正人[7]、藤井久男[8]、二見喜太郎[9]、舟山裕士[10]、根津理一郎[11]（東京女子医大IBDセンター外科[1]、横浜市立市民病院外科[2]、東北大学外科[3]、東京大学腫瘍外科[4]、新潟大学外科[5]、兵庫医科大学IBDセンター[6]、三重大学外科[7]、奈良医科大学外科[8]、福岡大学筑紫病院外科[9]、東北労災病院外科[10]、大阪労災病院外科[11]）

炎症性腸疾患における血栓症発症の頻度および危険因子に関する研究～多施設共同研究プロトコールの提案

○藤谷幹浩[1]、安藤勝祥[1]、伊藤貴博[1]、稲場勇平[1]、上野伸展[1]、富永素矢[1]、盛一健太郎[1]、田邊裕貴[1]、前本篤男[2,3]、蘆田知史[2,3]、高後　裕[1]（旭川医科大学内科学講座消化器・血液腫瘍制御内科学分野[1]、旭川医科大学消化管再生修復医学講座[2]、札幌東徳州会病院IBDセンター[3]）

〈コーヒーブレーク〉（15:15～15:30）

B-(4)-4　炎症性腸疾患患者の妊娠出産における現状とその対策（15:30～15:40）

総括　三浦総一郎　防衛医科大学校内科学講座（穂苅量太）

妊娠出産の転帰と治療内容に関する多施設共同研究の状況

三浦総一郎[1]、○穂苅量太[1]、高本俊介[1]、渡辺知佳子[1]、長堀正和[2]、渡辺　守[2]、松岡克善[3]、長沼　誠[3]、日比紀文[3]、本谷　聡[4]、樋田信幸[5]、松本誉之[5]、国崎玲子[6]、高橋宏和[6]、吉村直樹[7]、飯塚文瑛[8]、藤盛健二[9]、猿田雅之[10]、谷田諭史[11]、藤山佳秀[12]、内藤裕二[13]、渡辺憲治[14]、飯島英樹[15]、上野義隆[16]、田中信治[16]、石原俊治[17]、杉田　昭[18]、池上幸治[19]、松本主之[19]、仲瀬裕志[20]、岡崎和一[21]、石黒　陽[22]、松本吏弘[23]、嵜山敏男[24]、小林清典[25]、横山　薫[25]、松井敏幸[26]、鶴身小都絵[26]、加賀谷尚史[27]（防衛医科大学校内科学[1]、東京医科歯科大学消化器内科[2]、慶應義塾大学医学部消化器内科[3]、札幌厚生病院IBDセンター[4]、兵庫医科大学内科学下部消化管科[5]、横浜市立大学消化器内科[6]、社会保険中央総合病院内科[7]、東京女子医科大学IBDセンター（消化器内科）[8]、埼玉医科大学消化器肝臓内科[9]、慈恵会医科大学附属病院消化器・肝臓内科[10]、名古屋市立大学病院消化器内科[11]、滋賀医科大学消化器内科[12]、京都府立医科大学消化器内科[13]、大阪市立大学病院消化器内科[14]、大阪大学医学部附属病院消化器内科[15]、広島大学病院内視鏡診療科[16]、島根医科大学消化器内科[17]、横浜市立市民病院外科[18]、九州大学病院消化器内科[19]、京都大学医学部消化器内科[20]、関西医科大学消化器肝臓内科[21]、国立病院機構弘前病院消化器血液内科[22]、さいたま医療センター消化器科[23]、鹿児島大学医学部附属病院消化器内科[24]、

北里大学東病院消化器内科[25]、福岡大学筑紫病院消化器内科[26]、金沢大学附属病院消化器内科[27])

B-(4)-5　特殊な年齢層における炎症性腸疾患患者の治療指針の必要性　(15:40～16:00)

総括　三浦総一郎　防衛医科大学校内科学講座（穂苅量太）

高齢者炎症性腸疾患診療の現状把握 ―と前向き多施設共同研究の経過報告―

三浦総一郎[1]、○高本俊介[1]、穂苅量太[1]、渡辺知佳子[1]、田中浩紀[2]、本谷　聡[2]、加賀谷尚史[3]、松本史弘[4]、渡辺聡明[5]、吉村直樹[6]、長堀正和[7]、渡辺　守[7]、松岡克善[8]、日比紀文[8]、横山　薫[9]、小林清典[9]、谷田諭史[10]、馬場重樹[11]、藤山佳秀[11]、内藤裕二[12]、仲瀬裕志[13]、山上博一[14]、渡辺憲治[14]、石黒陽[15]、樋田信幸[16]、永井健太[17]、上野義隆[17]、田中信治[17]、石原俊治[18]、瀬戸山仁[19]、藤田　浩[19]、坪内博仁[19]、高橋晴彦[20]、松井敏幸[20]、二見喜太郎[21]、花井洋行[22]（防衛医科大学校内科[1]、札幌厚生病院IBDセンター[2]、金沢大学医学部消化器内科[3]、自治医科大学付属さいたま医療センター消化器科[4]、東京大学医学部　消化器内科[5]、社会保険中央総合病院内科[6]、東京医科歯科大学消化器内科[7]、慶應義塾大学医学部消化器内科[8]、北里大学東病院消化器内科[9]、名古屋市立大学病院消化器内科[10]、滋賀医科大学　消化器内科[11]、京都府立医科大学消化器内科[12]、京都大学医学部付属病院消化器内科[13]、大阪市立大学病院消化器内科[14]、国立病院機構弘前病院消化器内科[15]、兵庫医科大学内科学下部消化管科[16]、広島大学病院内視鏡診療科[17]、島根大学医学部消化器内科[18]、鹿児島大学医学部付属病院消化器内科[19]、福岡大学筑紫病院消化器内科[20]、福岡大学筑紫病院外科[21]、浜松南病院消化器病・IBDセンター[22])

小児期発症炎症性腸疾患の治療に関する全国調査

○清水俊明[1]、友政剛[2]、田尻　仁[3]、国崎玲子[4]、石毛　崇[5]、山田寛之[6]、新井勝大[7]、大塚宜一[1]、余田　篤[8]、牛島高介[9]、青松友槻[8]、永田　智[10]、内田恵一[11]、竹内一夫[12]（順天堂大学医学部小児科[1]、パルこどもクリニック[2]、大阪府立急性期・総合医療センター小児医療センター[3]、横浜市立大学附属市民総合医療センター[4]、群馬大学大学院医学系研究科小児科学[5]、大阪府立母子センター消化器内分泌科[6]、国立成育医療研究センター消化器科[7]、大阪医科大学泌尿生殖発達医学講座小児科[8]、久留米大学医療センター小児科[9]、順天堂大学静岡病院小児科[10]、三重大学医学部小児外科[11]、埼玉大学教育学部学校保健学講座[12])

B-(4)-2　炎症性腸疾患にともなう感染症の現状とその対策　(16:00～16:25)

総括　岡崎和一　関西医科大学　消化器・肝臓内科

我が国における炎症性腸疾患の急性増悪・再燃因子の前向き実態調査（特に感染症との関連性）

岡崎和一[1]、○大宮美香[1]、深田憲将[1]、佐々木誠[2]、渡辺憲治[3]、大川清孝[4]、加賀谷尚史[5]、高添正和[6]、酒匂美奈子[6]、渡辺守[7]、長堀正和[7]、飯塚文瑛[8]、後藤秀実[9]、谷田諭史[9]、花井洋行[10]、飯田貴之[10]、平田一郎[11]、藤田浩史[11]、加藤順[12]（関西医科大学内科学第三講座[1]、愛知医科大学消化器内科[2]、大阪市立大学消化器内科[3]、大阪市立十三市民病院[4]、金沢大学消化器内科[5]、社会保険中央総合病院IBDセンター[6]、東京医科歯科大学消化器内科[7]、東京女子医科大学IBDセンター[8]、名古屋市立大学消化器・代謝内科[9]、浜松南病院IBDセンター[10]、藤田保健衛生大学消化管内科[11]、和歌山県立医科大学第二内科[1])

炎症性腸疾患における免疫抑制療法中のB型肝炎再活性化に関する調査研究

坪内博仁[1]、○井戸章雄[1]、沼田政嗣[1]、森内昭博[1]、上村修司[1]、玉井　努[1]、船川慶太[1]、藤田　浩[1]、宇都浩文[1]、桶谷　眞[1]、嵜山敏男[2]、児玉眞由美[3]（鹿児島大学大学院消化器疾患・生活習慣病学、出水総合医療センター[2]、宮崎医療センター病院[3])

B-(3)　画期的な診断・治療の開発プロジェクト　ー治療面からー

B-(3)-1　難治性炎症性腸疾患に対する新規治療の位置づけ　(16:25～16:35)

総括　日比紀文　慶應義塾大学医学部消化器内科（渡辺　守）

潰瘍性大腸炎に対するtacrolimusとinfliximabの治療効果比較試験

○松岡克善[1]、長沼　誠[1]、金井隆典[1]、日比紀文[1]、渡辺　守[2]、樋田信幸[3]、松浦　稔[4]、猿田雅之[5]、朝倉敬子[6]（慶應義塾大学消化器内科[1]、東京医科歯科大学消化器病態学[2]、兵庫医科大学内科下部消化管科[3]、京都大学医学部消化

器内科[4]、東京慈恵会医科大学消化器・肝臓内科[5]、慶應義塾大学医学部衛生学公衆衛生学[6])

B-(3)-2　適切な免疫調節剤投与法、infliximab 二次無効例に対する対処(16:35～16:55)

新規多施設共同医師主導型臨床研究「アダリムマブと免疫調節剤併用中の寛解 CD 患者における免疫調節剤休薬の検討-Diamond2

○久松理一[1]、松本主之[2]、仲瀬裕志[3]、渡辺憲治[4]、渡辺　守[5]、日比紀文[1] (慶應義塾大学医学部消化器内科[1]、九州大学大学院病態機能内科学[2]、京都大学消化器内科[3]、大阪市立大学消化器内科[4]、東京医科歯科大学病態機能内科学[5])

クローン病に対するアダリムマブと免疫調節剤併用療法の検討：進捗状況

○松本主之[1]、仲瀬裕志[2]、渡辺憲治[3]、久松理一[4]、本谷　聡[5]、蘆田知史[6]、伊藤裕章[7]、鈴木康夫[8]、松本誉之[9]、松井敏幸[10]、日比紀文[4]、渡辺　守[11] (九州大学大学院病態機能内科学[1]、京都大学医学部消化器内科[2]、大阪市立大学大学院医学研究科消化器内科学[3]、慶應義塾大学医学部消化器内科[4]、JA 北海道厚生連札幌厚生病院 IBD センター[5]、札幌徳州会病院 IBD センター[6]、医療法人錦秀会インフュージョンクリニック[7]、東邦大学医療センター佐倉病院内科[8]、兵庫医科大学内科学下部消化管科[9]、福岡大学筑紫病院消化器内科[10]、東京医科歯科大学医学部消化器病態学[11])

事務局連絡

(17:00 終了予定)

懇親会 (17:00～)

Ⅳ．研究報告（続）

p-C）　基礎プロジェクト

C-(1)　診療に有用なバイオマーカー開発

C-(1)-1　免疫関連バイオマーカーの開発

総括　竹田　潔　大阪大学大学院医学系研究科（9:00～9:48）

ビタミンB9による腸管の炎症制御機構

○竹田　潔（大阪大学大学院医学系研究科免疫制御学）

IL-10 -/- 移入腸炎を用いたCXCR3阻害剤の役割

蓮井桂介[1]、○石黒　陽[2]、櫻庭裕丈[1]、平賀寛人[1]、福田眞作[1]（弘前大学医学部消化器血液内科[1]、国立病院機構弘前病院消化器血液内科[2]）

アポトーシス細胞の移入による腸管炎症抑制

○石原俊治、大嶋直樹、多賀育賢、岡　明彦、楠　龍策、園山浩紀、福庭暢彦、森山一郎、結城崇史、川島耕作、木下芳一（島根大学医学部内科学講座第二）

腸内細菌依存性腸炎モデルにおけるMyD88の細胞特異的役割について

○星　奈美子[1]、岩崎明子[2]、Ruslan Medzhitov[2]、　東　健[1]（神戸大学大学院医学研究科内科学講座消化器内科学分野[1]、Yale University School of Medicine, Department of Immunobiology[2]）

総括　千葉　勉　京都大学消化器内科（竹田　潔）（9:48～9:56）

dnTGF - βRII マウス大腸炎におけるIL-23, IL-17による制御機構

岡崎和一[1]、○安藤祐吾[1]、吉田勝紀[1]、常山幸一[2,3]、深田憲将[1]、松下光伸[1]、福井寿朗[1]、M. Eric Gershwin[2]（関西医科大学第三内科学講座、Division of Rheumatology, Allergy and Clinical Immunology, University of California at Davis、富山大学大学院医学薬学研究部病理診断学講座[3]）

腸炎惹起性RORgt-independent classical Th1細胞の発達分化

○三枝慶一郎、金井隆典、筋野智久、半田一己、三上洋平、林篤史、水野慎大、松本淳宏、木村佳代子、松岡克善、佐藤俊朗、久松理一、日比紀文（慶應義塾大学医学部消化器内科）

病原性メモリーCD4+T細胞を標的とした炎症性腸疾患根治療法開発の試み

○根本泰宏[1]、高原政宏[1]、金井隆典[2]、渡辺　守[1]（東京医科歯科大学消化器病態学[1]、慶應義塾大学医学部消化器内科[2]）

C-(1)-2　臨床的バイオマーカーの開発（9:56～10:12）

総括　日比紀文　慶應義塾大学医学部消化器内科（坪内博仁）

疾患活動性バイオマーカーとしてのMUC5ACの有効性　-難治性潰瘍性大腸炎での検討-

○溝下　勤、谷田諭史、城　卓志（名古屋市立大学大学院医学研究科消化器・代謝内科学）

CAP治療効果予測因子としての温感の意義とメカニズムについて

○ 飯塚政弘[1,2]、衛藤　武[2]、相良志穂[1]、沼田友華[3]、柳原　悠[3]、熊谷　誠[3]（秋田赤十字病院附属あきた健康管理センター[1]、秋田赤十字病院消化器科[2]、秋田赤十字病院臨床工学科[3]）

C-(1)-3　疾患特異的バイオマーカーの開発（10:12～10:28）

総括　坪内博仁　鹿児島大学大学院医歯学総合研究科消化器疾患・生活習慣病学

日本人のIBD感受性遺伝子

○有村佳昭[1]、一色裕之[1]、永石歓和[2]、苗代康可[3]、篠村恭久[1]、今井浩三[4]（札幌医科大学第一内科[1]、札幌医科大学第二解剖[2]、札幌医科大学医療人育成センター[3]、東京大学医科学研究所　附属病院　病院長[4]）

炎症性腸疾患における免疫寛容関連E3ユビキチン・リガーゼGRAILの関与

○飯島英樹、向井 章、新崎信一郎、井上隆弘、日山智史、白石衣里、川井翔一郎、辻井正彦、竹原徹郎（大阪大学大学院医学系研究科・消化器内科学）

C-(1)-4　腸内細菌関連バイオマーカーの開発　(10:28～10:49)

総括　藤山佳秀　滋賀医科大学消化器内科

クローン病患者腸内細菌叢におけるFaecalibacterium prausnitzii と硫酸還元菌の検討

○ 藤本剛英[1]、安藤 朗[1]、今枝広丞[2]、高橋憲一郎[1]、馬場重樹[2]、佐々木雅也[2]、辻川知之[2]、藤山佳秀[2]（滋賀医科大学大学院感染応答・免疫調節部門消化器免疫分野、滋賀医科大学消化器内科）

新規乳酸菌による腸炎改善作用のメカニズム解析および経口投与による腹部症状改善効果の検討

○藤谷幹浩[1]、上野伸展[1]、稲場勇平[1]、盛一健太郎[1]、田邊裕貴[1]、前本篤男[23]、蘆田知史[23]、高後　裕[1]（旭川医科大学内科学講座消化器・血液腫瘍制御内科学分野[1]、旭川医科大学消化管再生修復医学講座[2]、札幌東徳洲会病院IBDセンター[3]）

C-(1)-5　炎症による発癌バイオマーカーの開発　(10:49～11:26)

総括　味岡洋一　新潟大学院医歯学総合研究科分子診断病理学分野

潰瘍性大腸炎の炎症性発癌過程におけるDNA損傷応答の意義

○谷　優佑[1]、味岡洋一[1]、渡辺佳緒里[1]、岩井俊文[2]、山口尚之[1]（新潟大学大学院医歯学総合研究科　分子・診断病理学[1]、新潟大学大学院医歯学総合研究科　消化器一般外科分野[2]）

MSCによる腫瘍イニシエーション抑制機構の解明

○一色裕之[1]、有村佳昭[1]、永石歓和[2]、苗代康可[3]、篠村恭久[1]、今井浩三[4]（札幌医科大学第一内科[1]、札幌医科大学第二解剖[2]、札幌医科大学医療人育成センター[3]、東京大学医科学研究所　附属病院　病院長[4]）

低分子量GTP蛋白Ral の炎症性腸疾患関連大腸発癌における役割

○吉野琢哉[1]、仲瀬裕志[1]、千葉　勉[1]（京都大学医学研究科消化器内科学）

粘液産生がんにおけるAtoh1発現の意義

○土屋輝一郎、加納嘉人、鄭　秀、堀田伸勝、福島啓太、日比谷秀爾、根本泰宏、大島　茂、岡本隆一、永石宇司、中村哲也、渡辺　守（東京医科歯科大学消化器病態学）

C-(2)　粘膜修復機構解析と治療応用　(11:26～11:55)

総括　今井浩三　東京大学医科学研究所先端医療研究センター癌制御分野（有村佳昭）

腸炎における造血幹細胞と骨髄ニッチの異常

○永石歓和[2]、一色裕之[1]、有村佳昭[1]、苗代康可[3]、篠村恭久[1]、今井浩三[4]（札幌医科大学第一内科[1]、札幌医科大学第二解剖[2]、札幌医科大学医療人育成センター[3]、東京大学医科学研究所　附属病院　病院長[4]）

潰瘍性大腸炎における大腸上皮の創傷治癒に対するWnt5a short peptideの効果に関する検討

内藤裕二、髙木智久、○内山和彦（京都府立医科大学消化器内科）

腸管上皮幹細胞培養とその臨床応用技術開発

○中村哲也、油井史郎、水谷知裕、福田将義、野崎賢吾、根本泰宏、岡本隆一、土屋輝一郎、渡辺　守（東京医科歯科大学消化器病態学）

事務局連絡

閉会挨拶

(12:00終了予定)

Ⅶ.　研究成果の別刷

TECHNICAL REPORTS

nature medicine

Functional engraftment of colon epithelium expanded *in vitro* from a single adult Lgr5$^+$ stem cell

Shiro Yui[1,6], Tetsuya Nakamura[2,6], Toshiro Sato[3,5], Yasuhiro Nemoto[1], Tomohiro Mizutani[1], Xiu Zheng[1], Shizuko Ichinose[4], Takashi Nagaishi[1], Ryuichi Okamoto[2], Kiichiro Tsuchiya[1], Hans Clevers[3] & Mamoru Watanabe[1]

Adult stem-cell therapy holds promise for the treatment of gastrointestinal diseases. Here we describe methods for long-term expansion of colonic stem cells positive for leucine-rich repeat containing G protein-coupled receptor 5 (Lgr5$^+$ cells) in culture. To test the transplantability of these cells, we reintroduced cultured GFP$^+$ colon organoids into superficially damaged mouse colon. The transplanted donor cells readily integrated into the mouse colon, covering the area that lacked epithelium as a result of the introduced damage in recipient mice. At 4 weeks after transplantation, the donor-derived cells constituted a single-layered epithelium, which formed self-renewing crypts that were functionally and histologically normal. Moreover, we observed long-term (>6 months) engraftment with transplantation of organoids derived from a single Lgr5$^+$ colon stem cell after extensive *in vitro* expansion. These data show the feasibility of colon stem-cell therapy based on the *in vitro* expansion of a single adult colonic stem cell.

Epithelial stem cells maintain tissue homeostasis throughout the gastrointestinal tract[1–3]. The Wnt, bone morphogenetic protein (BMP) and Notch cascades function together to regulate stem-cell maintenance[4,5]. *Lgr5* marks stem cells in small intestinal and colonic crypts[6] and in gastric units[7]. *Bmi1* may mark distinct stem cells in the proximal small intestine[8]. It has been shown that freshly isolated intestinal epithelium can be transplanted in rodents after resident epithelium has been surgically removed[9,10]. We previously developed a three-dimensional culture technique that allows expansion of single Lgr5$^+$ stem cells from small intestine[11], stomach[7] and colon[12]. The resulting organoids then expand and self organize into an epithelial architecture that is reminiscent of that seen in *in vivo* histology. Moreover, the growing organoids maintain their tissue identity even after prolonged culture. Here we sought to evaluate whether the cultured Lgr5$^+$ cells faithfully represent the tissue-resident Lgr5$^+$ stem cells and, thus, are able to regenerate epithelial tissue *in vivo*. Considering that the colon is very vulnerable to disease in humans, we focused on colonic stem cells in our analyses.

RESULTS

Long-term, serum-free culture system for colonic organoids

We subjected the colons of adult mice to a combination of enzymes[13], reducing agents[14] and mechanical disruption. The resulting crypt fragments were mostly devoid of α smooth muscle actin gene (*Acta2*)-expression–positive non-epithelial components and consisted of a mix of cadherin 1, type 1, E-cadherin (*Cdh1*)$^+$ cells expressing terminal differentiation marker genes (*Muc2*, *CA2* and *ChgA*) and Lgr5$^+$ stem cells (**Supplementary Fig. 1a,b**).

The addition of R-spondin 1 (Rspo1), Noggin and epidermal growth factor (EGF), which are all essential to small intestine culture[11], did not maintain the growth of colonic crypts. We therefore developed the following 'TMDU (Tokyo Medical and Dental University) protocol': we embedded crypts in type I collagen in serum-free medium with Wnt3a, hepatocyte growth factor (HGF)[15,16] and BSA, in addition to Rspo1, Noggin and EGF (**Supplementary Fig. 1c**). Sequential imaging of the cultures revealed rapid growth of cystic structures (**Fig. 1a**). Wnt3a, Rspo1 and BSA were essential to this growth (**Supplementary Fig. 1d**). As predicted by previous results[17,18], Rspo1 could be substituted with Wnt3a (data not shown). Although Noggin, EGF and HGF were not essential for growth of the colonic crypts, each enhanced their growth (**Supplementary Fig. 1e**). The colonic organoids rarely had buds (**Fig. 1a, Supplementary Fig. 2a** and **Supplementary Video 1**). Of note, small intestinal organoids also generate cystic structures when Wnt3a is added to them[19].

The colonic organoids were single layered (**Supplementary Fig. 2b**), and all the cells within were positive for Cdh1 expression (**Fig. 1b**). The basal membranes of the organoids faced outward (**Fig. 1b**). Ki67$^+$ cells were present in the colonic organoids (**Fig. 1b**), as were alcian blue–positive goblet cells, chromogranin A (ChgA)$^+$ enteroendocrine cells, carbonic anhydrase II (CA2)$^+$ colonocytes and cytochrome c oxidase subunit I (COX1)$^+$ tuft cells[20] (**Fig. 1b**). Transmission electron microscopy revealed epithelial characteristics such as microvilli (**Fig. 1c**) and junctional complexes (**Fig. 1d**) in the organoids. However, stromal cells were absent (**Supplementary Fig. 2c**). Mitotic cells with condensed chromosomes were present in the organoids (**Fig. 1e**), and goblet cells (**Fig. 1f**) and enteroendocrine cells (**Fig. 1g**) could also be clearly detected.

[1]Department of Gastroenterology and Hepatology, Graduate School, Tokyo Medical and Dental University, Bunkyo-ku, Tokyo, Japan. [2]Department of Advanced Therapeutics for Gastrointestinal Diseases, Tokyo Medical and Dental University, Bunkyo-ku, Tokyo, Japan. [3]Hubrecht Institute and University Medical Centre, Utrecht, The Netherlands. [4]Research Center for Medical and Dental Sciences, Tokyo Medical and Dental University, Bunkyo-ku, Tokyo, Japan. [5]Present address: Department of Gastroenterology, Keio University School of Medicine, Shinjuku-ku, Tokyo, Japan. [6]These authors contributed equally to this work. Correspondence should be addressed to H.C. (h.clevers@hubrecht.eu) or M.W. (mamoru.gast@tmd.ac.jp).

Received 30 July 2011; accepted 29 November 2011; published online 11 March 2012; doi:10.1038/nm.2695

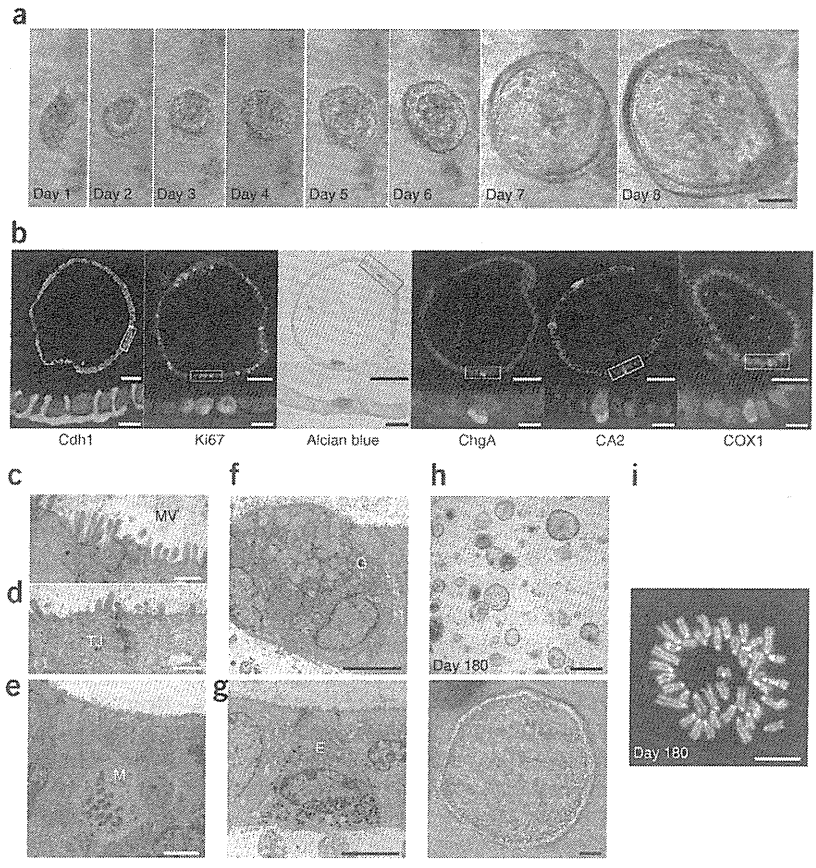

Figure 1 Long-term, serum-free culture of colonic epithelial cells. (**a**) A representative colonic crypt growing as a cystic structure. Scale bar, 50 μm. Time-lapse images of another colonic crypt are shown in **Supplementary Figure 2a** and **Supplementary Video 1**. (**b**) Histology of the colonic organoids at day 8 of culture. Cdh1$^+$ cells, actively proliferating Ki67$^+$ cells (green) and terminally differentiated cells stained with alcian blue (blue, goblet cells) or immunostained with ChgA (green, enteroendocrine cells), CA2 (green, colonocytes) or COX1 (green, tuft cells) are shown. Higher magnification views of the boxed areas are shown at the bottom. DAPI staining was performed, except for the experiments in which we performed alcian blue staining. Scale bars, top, 50 μm; bottom, 10 μm. (**c**–**g**) Transmission electron microscopy analysis for organoids at day 8. (**c**,**d**) Microvilli (MV) and intracellular tight junctions (TJ) are shown. (**e**) Mitotic (M) cells showing chromatin condensation. (**f**,**g**) Goblet cells (G) with mucus granules (**f**) and enteroendocrine cells (E) with electron dense granules (**g**) are shown. Scale bars: **c**,**d**, 0.5 μm; **e**–**g**, 5 μm. Low-power views of **f** and **g** are also shown in **Supplementary Figure 2c**. (**h**) The culture at day 180 (top) and its representative organoid (bottom). Scale bars, top, 500 μm; bottom, 50 μm. Images of the growth of a single cell after passage are shown in **Supplementary Figure 3** and **Supplementary Video 2**. (**i**) Metaphase spread of a cell at day 180 shows a normal karyotype ($2n = 40$). Scale bar, 10 μm.

The organoids could be passaged weekly at a 1:2 ratio (**Supplementary Fig. 3** and **Supplementary Video 2**). Addition of the Rho kinase inhibitor Y-27632 (ref. 21) improved the replating efficiency of the organoids[11]. We successfully propagated organoids for more than 6 months without clear alterations of morphology (**Fig. 1h**) or karyotype (**Fig. 1i**).

Lgr5$^+$ cells are enriched in colonic organoids

We tracked the expression of *Lgr5* over 60 d and found a substantial elevation during the first 8 d of observation (**Fig. 2a**). We found no change in the expression of *ChgA* and *CA2*, whereas *Muc2* expression was repressed in the first 8 d (**Fig. 2a**). Addition of a combination of Wnt3a, Rspo1 and BSA induced *Lgr5* expression (**Fig. 2b**). *Lgr5* expression was further upregulated by the addition of Noggin, which is an antagonist of BMP[22] (**Fig. 2b**). The Notch pathway suppresses the

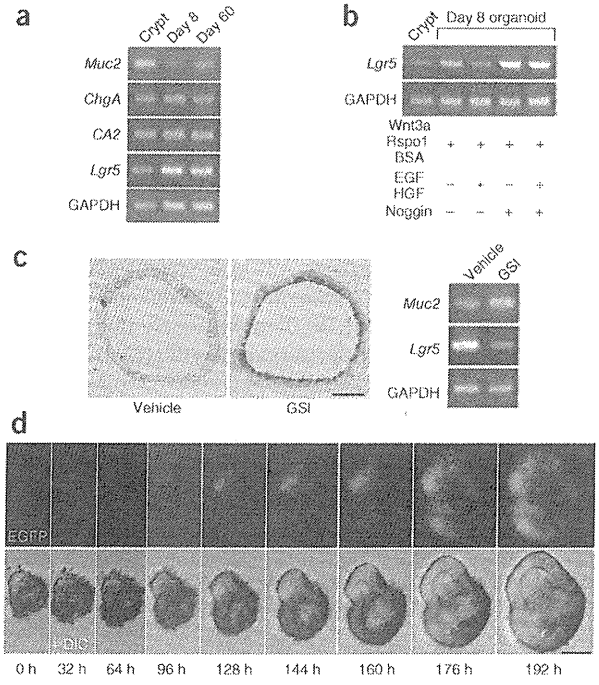

Figure 2 Lgr5$^+$ stem cells are enriched in cultured organoids. (**a**) RT-PCR analysis of the colonic crypts immediately after isolation (crypt) or organoids cultured for 8 or 60 d. *Lgr5* was upregulated and stayed constant thereafter. Differentiation marker genes (*Muc2*, *ChgA* and *CA2*) were expressed over 60 d. The primers used are listed in **Supplementary Table 1**. (**b**) RT-PCR shows that *Lgr5* upregulation is mediated by a combination of minimum factors (Wnt3a, Rspo1 and BSA) and Noggin but not by EGF and HGF. (**c**) Notch signal-mediated cell fate determination *in vitro*. Cultured organoids were treated with GSI, LY-411575 or vehicle alone from day 4 to day 8. Organoids stained with alcian blue are shown (left). Scale bar, 50 μm. RT-PCR shows that the expression of *Muc2* is upregulated, whereas the expression of *Lgr5* is reciprocally downregulated in organoids treated with LY-411575 (GSI, right). Similar results were obtained in three independent experiments, and representative data are shown. (**d**) A time-lapse imaging of a growing colonic crypt obtained from an *Lgr5-EGFP-ires-CreERT2* mouse over 192 h. The top panel shows EGFP and the bottom panel shows merged images of EGFP and differential interference contrast (DIC). Scale bar, 50 μm. The corresponding video (**Supplementary Video 3**) and similar results from another example are available as **Supplementary Figure 4a** and **Supplementary Video 4**.

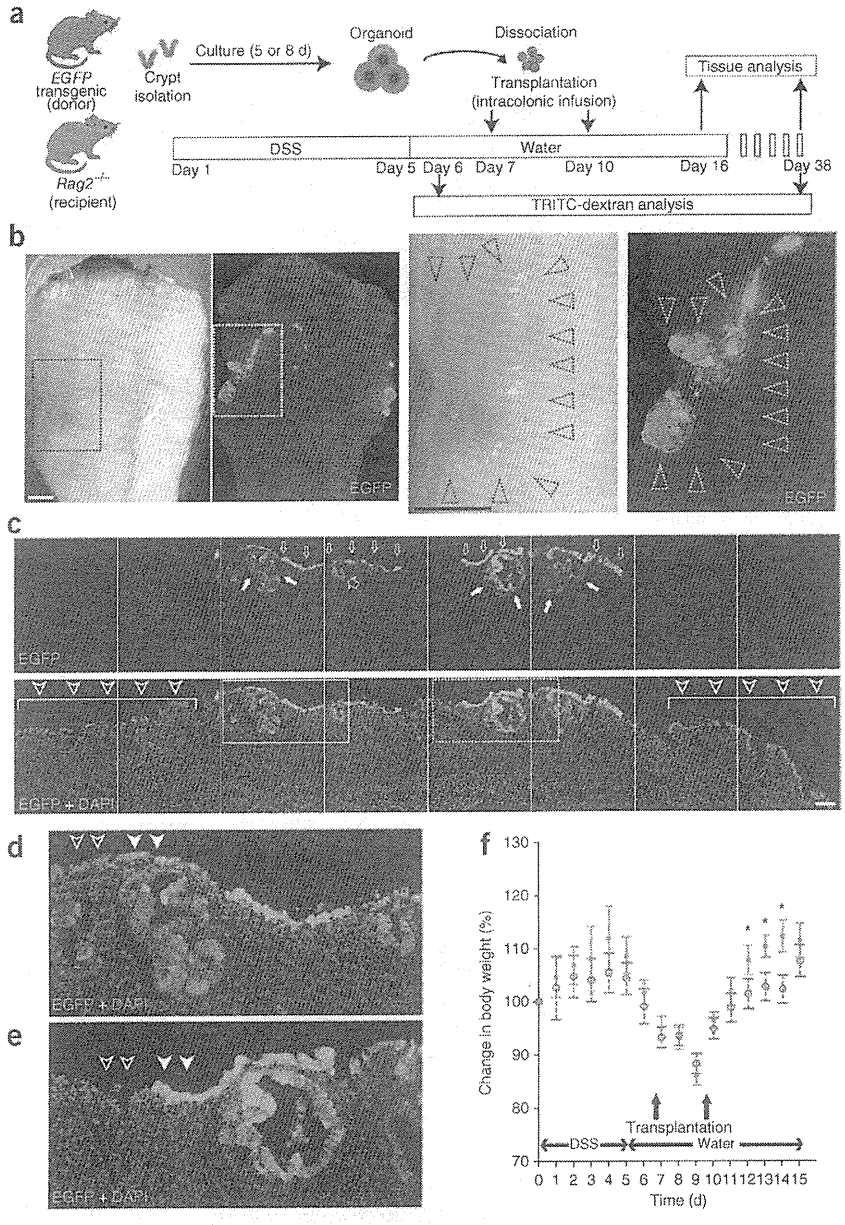

Figure 3 Transplantation of cultured cells improves acute colitis. (**a**) Experimental protocols. (**b**) Recipient colon at 6 d after transplantation. Low-power views (stereoscopic and fluorescent images) are shown on the left. High-power views of the areas in the dotted squares are shown in the right. The black dotted arrowheads show a depressed area surrounded by edematous mucosa. EGFP$^+$ areas overlapping the damaged region (white dotted arrowheads) are also shown. Note that the outline of the tissue is not precisely the same in the stereoscopic and fluorescent images, as they were acquired on different microscopes. Scale bars, 1 mm. (**c**) Histology of the EGFP$^+$ area shown in **b**. EGFP (top) and the merged image with DAPI staining (bottom). EGFP$^+$ cells cover the damaged mucosa that intervene separate areas preserving crypt structures (bottom, arrowheads). EGFP$^+$ cells constitute flat linings (top, narrow open arrow) or an invagination (top, wide open arrows), the latter of which is reminiscent of crypts. EGFP$^+$ cystic structures were also observed in the EGFP$^+$ cells (top, filled white arrows). The regions in the solid- and dotted-line boxes are shown at higher magnification in **d** and **e**, respectively. Scale bar, 100 μm. (**d**) High-power view of the solid box in **c**. (**e**) High-power view of the dotted box in **c**. (**f**) *Rag2*$^{-/-}$ mice were given DSS for 5 d, and then transplantation ($n = 6$) or sham-transplantion ($n = 6$) was performed. On day 16, the presence of engraftment was retrospectively assessed after the mice were killed. The body weights of the mice with EGFP$^+$ engraftment (green squares, $n = 4$) and sham-transplanted controls (red open circles, $n = 6$) are presented as a percentage of their initial weight. Error bars, s.e.m. $^*P < 0.05$ (Student's *t* test).

differentiation of progenitors[23,24] and stem cells[25] toward secretory lineages. We treated the colonic organoids with LY-411575, a γ-secretase inhibitor (GSI) that is capable of inhibiting Notch signaling[26,27]. Notch inhibition induced a goblet-cell phenotype with an increased level of *Muc2* mRNA and a reciprocal decrease in the expression of *Lgr5* (**Fig. 2c**).

We next performed live imaging of colonic organoids obtained from *Lgr5-EGFP-internal ribosome entry site (ires)-CreERT2* mice[6] in which an enhanced GFP (EGFP) and tamoxifen-inducible Cre recombinase cassette is integrated into the *Lgr5* locus. The *Lgr5*-promoter–driven EGFP expression initially stayed at a marginal level but then increased beginning at day 5 (**Fig. 2d**, **Supplementary Fig. 4a** and **Supplementary Videos 3** and **4**). We confirmed the expansion of Lgr5$^+$ cells at a single-cell resolution (**Supplementary Fig. 4b**). Over multiple passages, the *Lgr5-EGFP* locus tended to become silenced, whereas the wild-type *Lgr5* allele remained active (**Fig. 2a,b**). Taken together, colonic Lgr5$^+$ stem cells were able to self renew and expand *in vitro*.

Cultured colonic organoids rescue damaged epithelium

We next tested the transplantability of the cultured organoids (**Fig. 3a**). We induced colonic mucosal damage by providing immunocompromised *Rag2*$^{-/-}$ mice with colitis-inducing dextran sulfate sodium (DSS)[28] for 5 d. Most of the mice developed acute colitis characterized by weight loss, bloody stool, diarrhea and epithelial injury in the distal colon. At 7 and 10 d after initiating DSS administration, we dissociated the organoids cultured from *EGFP* transgenic mice[29] into small fragments, suspended them in a Matrigel-containing PBS and instilled them by enema in recipient mice.

At 16 d after the start of DSS administration, the recipient colons showed varying degrees of recovery. Multiple EGFP$^+$ areas appeared as well-demarcated patches in the treated colons (**Fig. 3b**). We did not observe any EGFP$^+$ areas in colons not treated with DSS (data not shown). Histologically, the EGFP$^+$ cells covered the submucosa and were located between the less damaged recipient tissues (**Fig. 3c**). The EGFP$^+$ cells formed flat or slightly invaginated linings (**Fig. 3c**). We also observed large cystic EGFP$^+$ structures below the surface of the treated colons (**Fig. 3c**). Some of the EGFP$^+$ areas connected to the recipients' epithelium (**Fig. 3d**), whereas others repopulated areas that were devoid of recipient epithelium (**Fig. 3e**). Notably, the body weights of the mice with engraftment were

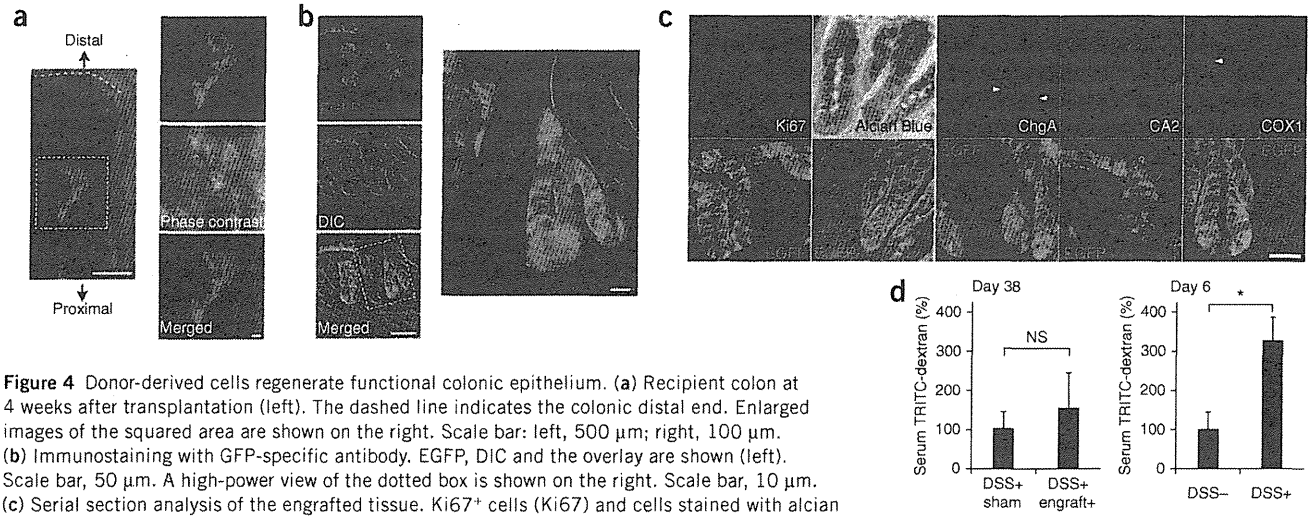

Figure 4 Donor-derived cells regenerate functional colonic epithelium. (**a**) Recipient colon at 4 weeks after transplantation (left). The dashed line indicates the colonic distal end. Enlarged images of the squared area are shown on the right. Scale bar: left, 500 μm; right, 100 μm. (**b**) Immunostaining with GFP-specific antibody. EGFP, DIC and the overlay are shown (left). Scale bar, 50 μm. A high-power view of the dotted box is shown on the right. Scale bar, 10 μm. (**c**) Serial section analysis of the engrafted tissue. Ki67$^+$ cells (Ki67) and cells stained with alcian blue (goblet cells) or immunostained for ChgA, CA2 and COX1 are shown. Images are shown with or without DAPI staining. The bottom row shows neighboring sections stained for GFP. Arrowheads point to ChgA$^+$ or COX1$^+$ cells. Scale bar, 50 μm. (**d**) After DSS colitis induction, transplantation ($n = 6$) or sham transplantation ($n = 6$) was performed. Mice were administered TRITC-dextran by gavage before killing on day 38. Four out of six colons in the transplanted group had EGFP$^+$ engraftment, and the serum TRITC concentration in these mice is shown (DSS+ engraft+; $n = 4$) as a percentage of that in the sham-transplanted group (DSS+ sham; $n = 6$). As a control, DSS colitis was induced (DSS+; $n = 6$) or uninduced (DSS–; $n = 6$) in *Rag2*$^{-/-}$ mice, and these mice were subjected for the same assay on day 6 without transplantation. Data are shown as a percentage of the concentrations in uninduced mice. Error bars, s.e.m. $^*P < 0.05$, NS, not significant (Student's *t* test).

higher than those of sham-transplanted mice (**Fig. 3f**; with statistically significant results at days 12, 13 and 14, $P < 0.05$).

At 4 weeks after transplantation, tube-like EGFP$^+$ crypts appeared in the distal colon (**Fig. 4a**) that were morphologically indistinguishable from the surrounding EGFP$^-$ epithelium (**Fig. 4b**). Notably, the engrafted crypts were entirely EGFP$^+$, indicating the presence of EGFP$^+$ stem cells (**Fig. 4b**). Cells in the lower part of the EGFP$^+$ crypts were normally Ki67$^+$, and the EGFP$^+$ crypts contained all

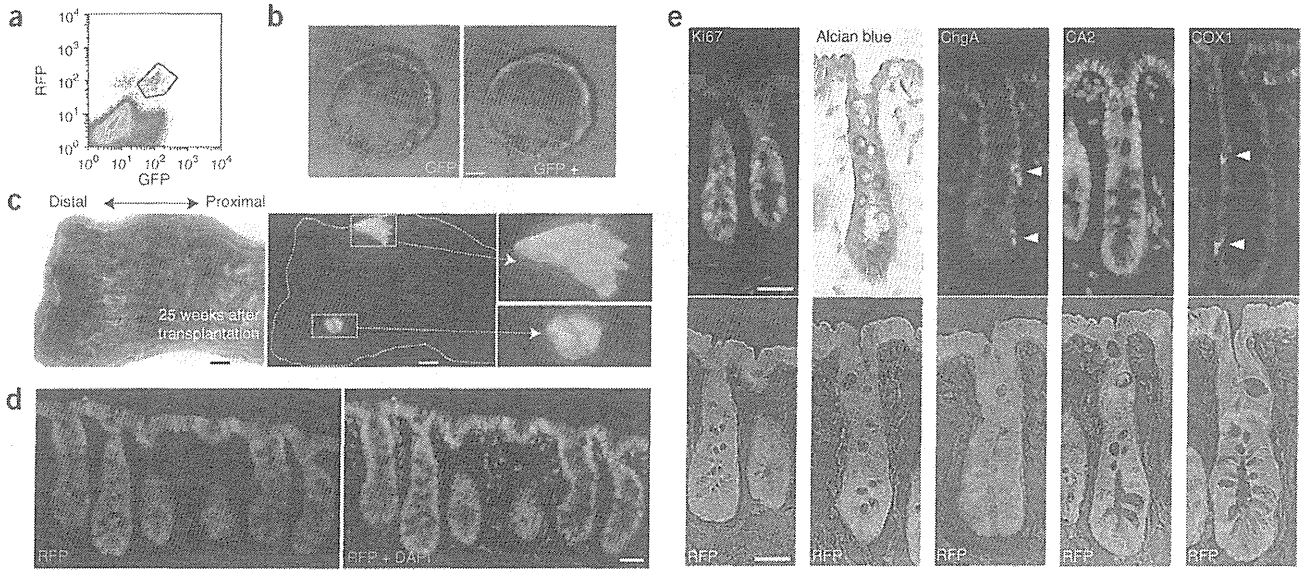

Figure 5 Single Lgr5$^+$ stem-cell–derived cultured cells serve as long-lived, multipotential stem cells *in vivo*. (**a**) Fluorescence-activated cell sorting analysis of colonic cells of *R26R-Confetti* mice crossed with *Lgr5-EGFP-ires-CreERT2* mice 3 d after Cre induction. The EGFP$^+$ and RFP$^+$ populations located in the box were sorted and cultured. (**b**) Images are shown of one out of four organoids grown from sorted single Lgr5$^+$ cells at day 6. EGFP$^+$ stem cells are scattered in the organoid (left), with all the offspring being positive for RFP (right). Scale bar, 50 μm. (**c**) Images of the recipient colon at 25 weeks after transplantation. The phase-contrast view of the recipient colon is shown on the left. The fluorescent image shows the tissue contains RFP$^+$ grafts (right). Scale bar, 1 mm. Enlarged images of the boxed areas are also shown (2.7-fold magnification). (**d**) Immunostaining of the RFP$^+$ engraft at 25 weeks after transplantation. An image of RFP-specific antibody staining (left) and an image of RFP staining merged with DAPI staining (right) are shown. Scale bar, 50 μm. (**e**) Serial section analysis of the engrafted RFP$^+$ tissue at 25 weeks after transplantation. The top panels show Ki67, alcian blue, ChgA, CA2 or COX1 staining with or without nuclei stained by DAPI. The bottom panels show the adjacent sections stained for RFP. Arrowheads point to ChgA$^+$ enteroendocrine cells and COX1$^+$ tuft cells. Scale bars, 50 μm.

terminally differentiated cell types (**Fig. 4c**). We probed the epithelial permeability of the engrafts using tetramethylrhodamine isothiocyanate (TRITC)-conjugated dextran (TRITC-dextran). Blood TRITC concentrations in transplanted mice were comparable to those in control mice, indicating a maintenance of epithelial barrier function in these engrafts (**Fig. 4d**). Notably, transplantation was less successful with freshly isolated donor cells ($P < 0.05$, Mann-Whitney U test; **Supplementary Fig. 5**), suggesting that the expansion of stem cells during the culture is associated with a higher success rate of transplantation. In addition, Matrigel-containing organoid suspensions transplanted better than organoids suspended in PBS (**Supplementary Fig. 5**; $P < 0.05$, Mann-Whitney U test), proposing a role for the simultaneous supply of extracellular matrix in successful transplantation.

Engraftment of organoids derived from a single Lgr5$^+$ cell

We next sought to initiate the protocol described above from a single stem cell (**Supplementary Fig. 6a**). We crossed *Lgr5-EGFP-ires-CreERT2* mice with *R26R-Confetti* reporter mice[30]. In the resulting offspring, tamoxifen-induced Cre activation resulted in Cre-mediated recombination at the *Rosa26* locus in individual Lgr5$^+$ stem cells, leading to stochastically selected expression of one out of four fluorescent proteins: red fluorescent protein (RFP), cyan fluorescent protein (CFP), GFP or yellow fluorescent protein (YFP). At 3 d after Cre activation, we sorted cells double positive for Lgr5-EGFP and Confetti-RFP, which consisted of ~0.02% of the total cells (**Fig. 5a**), equivalent to ~100 cells per mouse.

We cultured the sorted cells after a limiting dilution (100 cells per 96 well) using the Hubrecht protocol (Online Methods; protocol described previously[12] with addition of Y-27632 in the first 2 d). Four stem cells double positive for Lgr5-EGFP and Confetti-RFP grew out, which was comparable to the culture efficiency of small intestinal stem cells[11] (**Fig. 5b**). Organoids were expanded to more than 100 wells in >10 weeks, frozen and shipped. After thawing, we recovered the cells under the TMDU protocol. We transplanted ~500 organoids per recipient mouse, as described above. Analyses at 4, 17, 21 and 25 weeks after transplantation revealed the presence of grafts in these mice (**Fig. 5c** and **Supplementary Figs. 6b,c** and **7a**). At 25 weeks after transplantation, RFP$^+$ cells still generated a single-layered epithelium. We noted no sign of adenomatous or dysplastic change in any of the transplanted areas (**Fig. 5d**). Again, all differentiated cell types, as well as Ki67$^+$ proliferating cells, were present at normal ratios (**Fig. 5e** and **Supplementary Fig. 7b**).

DISCUSSION

Here we describe methodologies to isolate, culture and transplant Lgr5$^+$ colon stem cells. Our observations confirm that *Lgr5* marks genuine stem cells that retain their self-renewal and multilineage-differentiation properties even after prolonged culture. A major difference between small-intestinal and colon-culture conditions is in the latter's requirement for Wnt. Although Wnt factors can initiate Wnt signals on their own, R-spondins (such as Rspo1) can only augment preexisting Wnt signals[31]. Because Paneth cells produce Wnt3, they serve as the center of organization of the stem cell niche[19]. At the colon crypt bottoms, secretory cells are located between the Lgr5$^+$ stem cells that—like Paneth cells—express CD24 (ref. 19). However, these CD24$^+$ secretory cells do not produce a sufficient amount of Wnt proteins *in vitro* (data not shown). Therefore, colon organoids cannot grow from Rspo1 alone but, rather, also require exogenous Wnt.

This study provides proof of principle that cultured Lgr5$^+$ cells can be used for stem-cell therapy to repair damaged epithelium. Transplanted cells adhere to and cover superficially damaged tissue. Further, engrafted recipient mice had higher body weights than ungrafted controls, implying a beneficial role for the donor cells in DSS-induced acute colitis. Although further optimization is clearly needed, the current study implies that *in vitro* expansion and transplantation of gastrointestinal stem cells may be a promising option for patients with severe gastrointestinal epithelial injuries.

Lgr5$^+$ stem cells divide once every day *in vivo*[6], thus defying the Hayflick limit[32]. They appear similarly unrestricted in their proliferative capacity *in vitro*, while they retain their original tissue identity. It is of interest that the Lgr5 protein is now known to reside in the Wnt receptor complex to function as a receptor for Rspo1 (refs. 33,34), which is a crucial component of long-term organoid culture systems that we have developed. As the resulting organoids have now been proven to be transplantable, the Lgr5$^+$ stem cell isolation and expansion technology may provide a simple and safe avenue for the development of new regenerative and gene-therapy strategies.

METHODS

Methods and any associated references are available in the online version of the paper at http://www.nature.com/naturemedicine/.

Note: Supplementary information is available on the Nature Medicine website.

ACKNOWLEDGMENTS

We thank M. Okabe (Osaka University) for EGFP transgenic mice and Y. Kato, J. Inazawa, I. Sekiya (TMDU), H. Snippert and R. Vries (Hubrecht Institute) for technical assistance. This study was supported by Grant-in-Aid for Scientific Research from the Japanese Ministry of Education, Culture, Sports, Science and Technology, by the Health and Labour Sciences Research Grants for Research on Intractable Diseases from Ministry of Health, Labour and Welfare of Japan, and by a grant from the European Research Council and from the Dutch Cancer Foundation.

AUTHOR CONTRIBUTIONS

T. Nakamura, H.C. and M.W. designed the study. S.Y., T. Nakamura and T.S. performed experiments and analyzed data. T. Nakamura, T.S. and H.C. wrote the paper. Y.N., T. Nagaishi and K.T. assisted in transplantation experiments. T.M., X.Z. and K.T. gave support in gene analysis. R.O. helped with the immunohistochemistry. S.I. advised on the electron microscopy. H.C. and M.W. gave conceptual advice and supervised the project.

COMPETING FINANCIAL INTERESTS

The authors declare competing financial interests: details accompany the full-text HTML version of the paper at http://www.nature.com/naturemedicine/.

Published online at http://www.nature.com/naturemedicine/.
Reprints and permissions information is available online at http://www.nature.com/reprints/index.html.

1. Potten, C.S., Booth, C. & Pritchard, D.M. The intestinal epithelial stem cell: the mucosal governor. *Int. J. Exp. Pathol.* **78**, 219–243 (1997).
2. Bjerknes, M. & Cheng, H. Intestinal epithelial stem cells and progenitors. *Methods Enzymol.* **419**, 337–383 (2006).
3. Barker, N., van de Wetering, M. & Clevers, H. The intestinal stem cell. *Genes Dev.* **22**, 1856–1864 (2008).
4. Crosnier, C., Stamataki, D. & Lewis, J. Organizing cell renewal in the intestine: stem cells, signals and combinatorial control. *Nat. Rev. Genet.* **7**, 349–359 (2006).
5. Radtke, F. & Clevers, H. Self-renewal and cancer of the gut: two sides of a coin. *Science* **307**, 1904–1909 (2005).
6. Barker, N. *et al.* Identification of stem cells in small intestine and colon by marker gene *Lgr5*. *Nature* **449**, 1003–1007 (2007).
7. Barker, N. *et al.* Lgr5^{+ve} stem cells drive self-renewal in the stomach and build long-lived gastric units *in vitro*. *Cell Stem Cell* **6**, 25–36 (2010).
8. Sangiorgi, E. & Capecchi, M.R. *Bmi1* is expressed *in vivo* in intestinal stem cells. *Nat. Genet.* **40**, 915–920 (2008).
9. Avansino, J.R., Chen, D.C., Woolman, J.D., Hoagland, V.D. & Stelzner, M. Engraftment of mucosal stem cells into murine jejunum is dependent on optimal dose of cells. *J. Surg. Res.* **132**, 74–79 (2006).
10. Tait, I.S., Evans, G.S., Flint, N. & Campbell, F.C. Colonic mucosal replacement by syngeneic small intestinal stem cell transplantation. *Am. J. Surg.* **167**, 67–72 (1994).

11. Sato, T. *et al.* Single Lgr5 stem cells build crypt-villus structures *in vitro* without a mesenchymal niche. *Nature* **459**, 262–265 (2009).
12. Sato, T. *et al.* Long-term expansion of epithelial organoids from human colon, adenoma, adenocarcinoma, and Barrett's epithelium. *Gastroenterology* **141**, 1762–1772 (2011).
13. Booth, C., Patel, S., Bennion, G.R. & Potten, C.S. The isolation and culture of adult mouse colonic epithelium. *Epithelial Cell Biol.* **4**, 76–86 (1995).
14. Whitehead, R.H., Demmler, K., Rockman, S.P. & Watson, N.K. Clonogenic growth of epithelial cells from normal colonic mucosa from both mice and humans. *Gastroenterology* **117**, 858–865 (1999).
15. Kanayama, M. *et al.* Hepatocyte growth factor promotes colonic epithelial regeneration via Akt signaling. *Am. J. Physiol. Gastrointest. Liver Physiol.* **293**, G230–G239 (2007).
16. Tahara, Y. *et al.* Hepatocyte growth factor facilitates colonic mucosal repair in experimental ulcerative colitis in rats. *J. Pharmacol. Exp. Ther.* **307**, 146–151 (2003).
17. Kim, K.A. *et al.* Mitogenic influence of human R-spondin1 on the intestinal epithelium. *Science* **309**, 1256–1259 (2005).
18. Wei, Q. *et al.* R-spondin1 is a high affinity ligand for LRP6 and induces LRP6 phosphorylation and β-catenin signaling. *J. Biol. Chem.* **282**, 15903–15911 (2007).
19. Sato, T. *et al.* Paneth cells constitute the niche for Lgr5 stem cells in intestinal crypts. *Nature* **469**, 415–418 (2011).
20. Gerbe, F. *et al.* Distinct ATOH1 and Neurog3 requirements define tuft cells as a new secretory cell type in the intestinal epithelium. *J. Cell Biol.* **192**, 767–780 (2011).
21. Watanabe, K. *et al.* A ROCK inhibitor permits survival of dissociated human embryonic stem cells. *Nat. Biotechnol.* **25**, 681–686 (2007).
22. Haramis, A.P. *et al.* *De novo* crypt formation and juvenile polyposis on BMP inhibition in mouse intestine. *Science* **303**, 1684–1686 (2004).
23. Fre, S. *et al.* Notch signals control the fate of immature progenitor cells in the intestine. *Nature* **435**, 964–968 (2005).
24. van Es, J.H. *et al.* Notch/γ-secretase inhibition turns proliferative cells in intestinal crypts and adenomas into goblet cells. *Nature* **435**, 959–963 (2005).
25. van Es, J.H., de Geest, N., van de Born, M., Clevers, H. & Hassan, B.A. Intestinal stem cells lacking the Math1 tumour suppressor are refractory to Notch inhibitors. *Nat. Commun.* **1**, 18 (2010).
26. Wong, G.T. *et al.* Chronic treatment with the γ-secretase inhibitor LY-411,575 inhibits β-amyloid peptide production and alters lymphopoiesis and intestinal cell differentiation. *J. Biol. Chem.* **279**, 12876–12882 (2004).
27. Okamoto, R. *et al.* Requirement of Notch activation during regeneration of the intestinal epithelia. *Am. J. Physiol. Gastrointest. Liver Physiol.* **296**, G23–G35 (2009).
28. Wirtz, S., Neufert, C., Weigmann, B. & Neurath, M.F. Chemically induced mouse models of intestinal inflammation. *Nat. Protoc.* **2**, 541–546 (2007).
29. Okabe, M., Ikawa, M., Kominami, K., Nakanishi, T. & Nishimune, Y. 'Green mice' as a source of ubiquitous green cells. *FEBS Lett.* **407**, 313–319 (1997).
30. Snippert, H.J. *et al.* Intestinal crypt homeostasis results from neutral competition between symmetrically dividing Lgr5 stem cells. *Cell* **143**, 134–144 (2010).
31. Binnerts, M.E. *et al.* R-Spondin1 regulates Wnt signaling by inhibiting internalization of LRP6. *Proc. Natl. Acad. Sci. USA* **104**, 14700–14705 (2007).
32. Hayflick, L. & Moorhead, P.S. The serial cultivation of human diploid cell strains. *Exp. Cell Res.* **25**, 585–621 (1961).
33. de Lau, W. *et al.* Lgr5 homologues associate with Wnt receptors and mediate R-spondin signalling. *Nature* **476**, 293–297 (2011).
34. Carmon, K.S., Gong, X., Lin, Q., Thomas, A. & Liu, Q. R-spondins function as ligands of the orphan receptors LGR4 and LGR5 to regulate Wnt/β-catenin signaling. *Proc. Natl. Acad. Sci. USA* **108**, 11452–11457 (2011).

ONLINE METHODS

Mice. *Rag2*$^{-/-}$ mice were from Taconic Farms and Central Laboratories for Experimental Animals. *EGFP* transgenic mice[29], *Lgr5-EGFP-ires-CreERT2* mice[6] and *R26R-Confetti* mice[30] are described elsewhere. Male and female mice were randomly used for all experiments. All animal experiments were performed with the approval of the Institutional Animal Care and Use Committee of TMDU.

TMDU protocol for crypt isolation and three-dimensional culture. The colonic tissue was minced and digested. The crypts were further purified by mechanical disruption and density gradient centrifugation. A total of 2,000 crypts were suspended in 200 µl of the collagen type I solution (Nitta Gelatin Inc.) and placed in 48-well plates. After polymerization, 500 µl of Advanced DMEM/F12 containing BSA (Sigma), mouse EGF (mEGF) (PeproTech), mWnt3a, mRspo1, mHGF and mNoggin (all from R&D Systems) was added (TMDU medium). For passage, the gel was digested, and then the organoids were disaggregated with EDTA. The dissociated organoids were mixed in type I collagen solution and used for culture. A Rho kinase inhibitor, Y-27632, was added for the first 2 d after the cells were propagated. Where indicated, to induce goblet cell differentiation, organoids were treated with LY-411575, a GSI. See details in the **Supplementary Methods**.

Chromosome analysis. Chromosome karyotyping was performed according to a standard protocol as detailed in the **Supplementary Methods**.

Stereomicroscopy, phase-contrast imaging and histology. Images were acquired on either a fluorescence microscope equipped with phase-contrast setting (BZ-8000, KEYENCE), a fluorescent stereomicroscope system MVX10 (Olympus) or a fluorescence microscope DeltaVision system (Applied Precision). For histology and immunohistochemistry, tissues and organoids were fixed, sequentially dehydrated in sucrose in PBS, and frozen in OCT compound (Tissue Tek). Cryosections were examined by conventional H&E, alcian blue staining and a spectrum of immunohistochemical reactions, as detailed in the **Supplementary Methods**.

Transmission electron microscopy. Transmission electron microscopy was performed in a standard fashion and is detailed in the **Supplementary Methods**.

Live imaging. Live imaging was performed on the DeltaVision system. A culture dish placed on the microscope stage was covered with a chamber in which a humidified premixed gas consisting of 5% CO_2 and 95% air was infused, and the whole setup was set at 37 °C. DIC and fluorescent images were acquired at 20-min intervals. The data were processed using Softworx (Applied Precision) and, if necessary, image editing was performed using Adobe Photoshop Elements 7.0.

Semi-quantitative RT-PCR. Semi-quantitative RT-PCR was performed in standard fashion. The primer sequences used are listed in **Supplementary Table 1**. PCR products were separated on agarose gels and visualized using ImageQuant TL system (GE Healthcare).

Sorting and Hubrecht-protocol culture for single Lgr5^{+} cells. Tamoxifen was injected into *R26R-Confetti* mice crossed with *Lgr5-EGFP-ires-CreERT2* mice, and the colonic crypts from the resulting mice were isolated 3 d later. Epithelial cells were dissociated with TrypLE express (Invitrogen) and analyzed by MoFlo (DakoCytomation). Viable single cells were gated, and then the cells doubly positive for EGFP and RFP were sorted and embedded in Matrigel (BD Bioscience) on 96-well plates. An Advanced DMEM/F12 culture medium supplemented with penicillin and streptomycin, 4-(2-hydroxyethyl)-1-piperazineethanesulfonic acid (HEPES), glutamax, N2, B27 (all from Invitrogen) and growth factors (EGF, noggin and R-spondin) was diluted 1:1 with Wnt3a-conditioned medium and used as Hubrecht medium. Y-27632 was included for the first 2 d to avoid anoikis. Growth factors were added every other day, and the entire medium was changed every 4 d. See the **Supplementary Methods** for additional details.

Transplantation experiments. For the EGFP^{+} cell transplantations, cells isolated from colon tissues were cultured for 5 or 8 d according to the TMDU protocol and used as donor cells. For single Lgr5^{+}-cell–derived organoid transplantation, cells were expanded based on the Hubrecht protocol and then cryopreserved. The cells were then shipped, thawed and further cultured. Acute colitis was induced by feeding 6-week-old *Rag2*$^{-/-}$ mice with 3.0% DSS (molecular weight 10,000; Ensuiko Sugar Refining Co.) dissolved in drinking water for 5 d (days 1–5). At 7 and 10 d after the start of DSS administration, donor cells equivalent to those from ~500 organoids were instilled into colonic lumen as a suspension. After infusion, the anal verge was glued for 6 h. After the transplantation on day 10, mice were maintained as usual before they were killed and analyzed. See the **Supplementary Methods** for additional details.

TRITC-dextran permeability assay. Intestinal permeability was assessed by enteral administration of TRITC-dextran (molecular mass 4.4 kDa; Sigma). Transplanted or sham-transplanted mice were gavaged with TRITC-dextran 4 h before killing on day 38. Whole blood was obtained at the time of killing, and then the colonic tissues were examined for whether the EGFP^{+} engrafts were present. TRITC-dextran measurements were performed on an ARVO MX (PerkinElmer), with serial dilutions of TRITC-dextran used as a standard curve.

Statistical analyses. Data are shown as means ± s.e.m. Data for **Figures 3f**, **4d** and **Supplementary Figure 7b** were statistically analyzed by the two-sample Student's *t* test. The data for **Supplementary Figure 5** showed non-normal distributions and were analyzed by Mann-Whitney *U* test. Statistical significance for comparisons was assigned at $P < 0.05$.

Additional methods. Detailed methodology is described in the **Supplementary Methods**.

CCL2-Induced Migration and SOCS3-Mediated Activation of Macrophages Are Involved in Cerulein-Induced Pancreatitis in Mice

KEITA SAEKI,* TAKANORI KANAI,* MASARU NAKANO,* YUJI NAKAMURA,* NAOTERU MIYATA,* TOMOHISA SUJINO,* YOSHIYUKI YAMAGISHI,* HIROTOSHI EBINUMA,* HIROMASA TAKAISHI,* YUUICHI ONO,* KAZUYOSHI TAKEDA,§ SHIGENARI HOZAWA,* AKIHIKO YOSHIMURA,‡ and TOSHIFUMI HIBI*

*Department of Gastroenterology and Hepatology, and ‡Department of Microbiology and Immunology, Keio University School of Medicine, Tokyo, Japan; and §Department of Immunology, Juntendo University School of Medicine, Tokyo, Japan

BACKGROUND & AIMS: Acute pancreatitis is a common inflammatory disease mediated by damage to acinar cells and subsequent pancreatic inflammation with recruitment of leukocytes. We investigated the pathologic roles of innate immune cells, especially macrophages, in cerulein– and L-arginine–induced acute pancreatitis in mice. **METHODS:** Acute pancreatitis was induced by sequential peritoneal administration of cerulein to mice. We determined serum concentrations of amylase and lipase, pancreatic pathology, and features of infiltrating mononuclear cells. We performed parabiosis surgery to assess the hemodynamics of pancreatic macrophages. **RESULTS:** Almost all types of immune cells, except for $CD11b^{high}CD11c^{-}$ cells, were detected in the pancreas of healthy mice. However, activated $CD11b^{high}CD11c^{-}$ cells, including $Gr\text{-}1^{low}$ macrophages and $Gr\text{-}1^{high}$ cells (granulocytes and myeloid-derived suppressor cells), were detected in damaged pancreas after cerulein administration. $CCL2^{-/-}$ mice given cerulein injections developed significantly less severe pancreatitis, with less infiltration of $CD11b^{high}CD11c^{-}Gr\text{-}1^{low}$ macrophages, but comparable infiltration of myeloid-derived suppressor cells, compared with cerulein-injected wild-type mice. Parabiosis and bone marrow analyses of these mice revealed that the $CD11b^{high}CD11c^{-}Gr\text{-}1^{low}$ macrophages had moved out of the bone marrow. Furthermore, mice with macrophage-specific deletion of suppressor of cytokine signaling 3 given injections of cerulein developed less severe pancreatitis and $Gr\text{-}1^{low}$ macrophage produced less tumor necrosis factor-α than wild-type mice given cerulein, although the absolute number of $CD11b^{high}CD11c^{-}Gr\text{-}1^{low}$ macrophages was comparable between strains. Induction of acute pancreatitis by L-arginine required induction of macrophage migration by CCL2, via the receptor CCR2. **CONCLUSIONS: Cerulein induction of pancreatitis in mice involves migration of $CD11b^{high}CD11c^{-}Gr\text{-}1^{low}$ macrophage from the bone marrow (mediated by CCL2 via CCR2) and suppressor of cytokine signaling 3–dependent activation of macrophage. These findings might lead to new therapeutic strategies for acute pancreatitis.**

Keywords: Immune Response; Signaling; Mouse Model; Chemokine.

Severe acute pancreatitis is an intractable disease. It has a mortality rate of approximately 20% because of severe complications, such as systemic inflammatory syndrome, acute respiratory distress syndrome, and renal failure, and requires intensive care treatments.[1,2] The pathogenesis of acute pancreatitis begins in an autodigestive manner.[3] Trypsinogen activation by cathepsin B[3] and autophagy via Atg5 activation[4,5] are involved in the primary pathogenesis and lead to subsequent autodigestion. Based on these findings, a number of randomized controlled studies have assessed various protease inhibitors for the treatment of human acute pancreatitis.[6–8] Unfortunately, no significant reduction in mortality was achieved. Activation of proteases is not solely responsible for the initiation of acute pancreatitis associated with the high mortality, and subsequent inflammation might also be critically involved.[9,10]

In this regard, it has been reported that macrophages,[11] granulocytes,[12] and $CD4^{+}$ T cells[13] are involved in the pathogenesis of acute pancreatitis, and it has been suggested that chemokines produced by injured acinar cells attract these immune cells to the pancreas.[14] With this background, we used a cerulein-induced pancreatitis model[15,16] in the present study to comprehensively clarify the types of macrophages/mononuclear phagocytes involved in the pathogenesis of acute pancreatitis and the mechanisms of their recruitment and activation.

Materials and Methods

Detailed methods are described in the Supplementary Materials and Methods.

Induction of Acute Pancreatitis

Cerulein (Sigma-Aldrich, St Louis, MO) was dissolved in phosphate-buffered saline (PBS) and administered intraperito-

Abbreviations used in this paper: APC, antigen-presenting cell; BM, bone marrow; cDC, classical dendritic cells; cKO, conditional knockout; IL, interleukin; L-Arg, L-arginine; LPS, lipopolysaccharide; MDSC, myeloid-derived suppressor cell; NF-κB, nuclear factor–κB; NK, natural killer; NKT, natural killer T cell; PBS, phosphate-buffered saline; RAG-2, recombinase-activated gene-2; SOCS, suppressor of cytokine signaling; STAT, signal transducer and activation of transcription; TCR, T-cell receptor; TNF-α, tumor necrosis factor–α; WT, wild-type.

0016-5085/$36.00
doi:10.1053/j.gastro.2011.12.054

BASIC AND TRANSLATIONAL PANCREAS

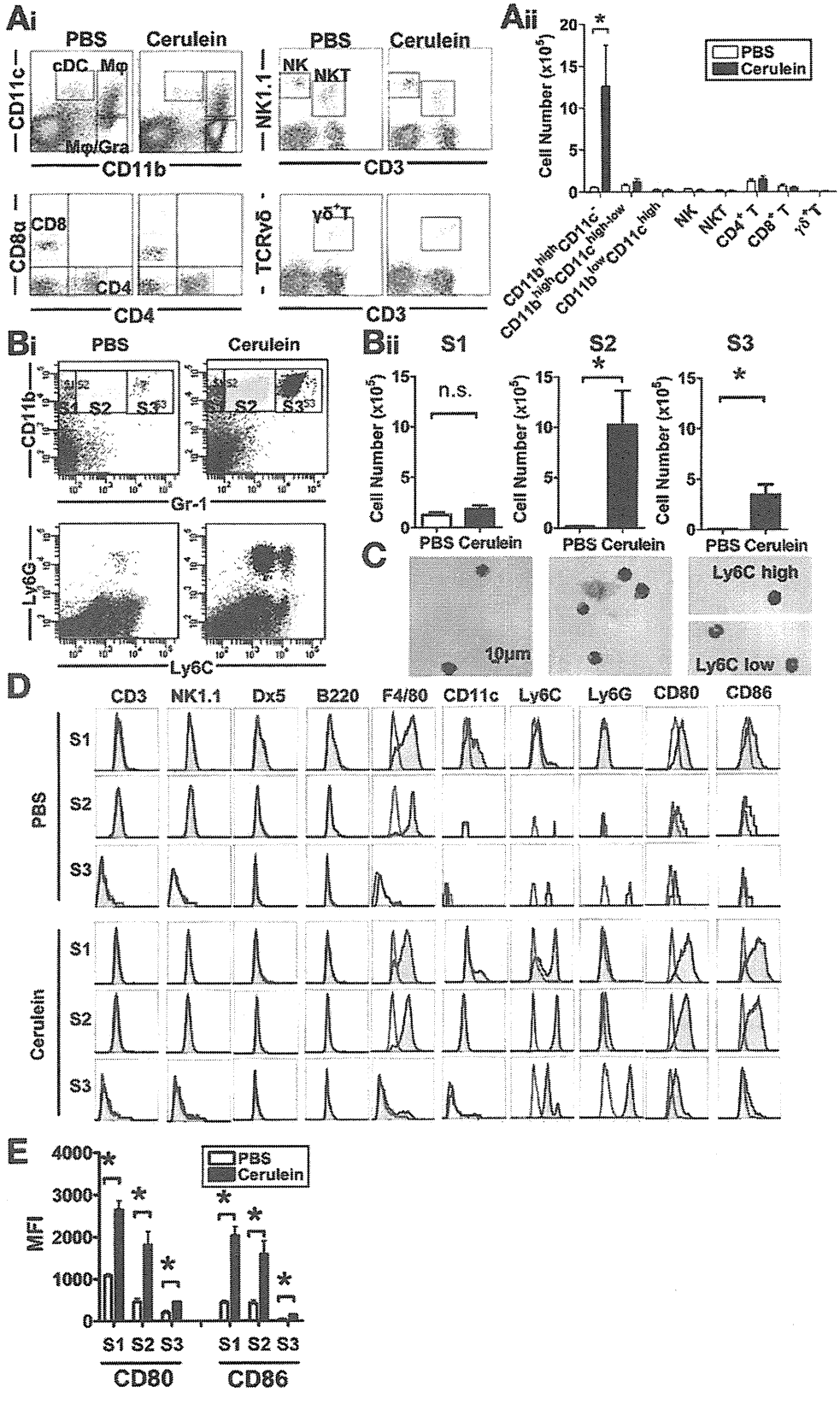
Ai
PBS
Cerulein
CD11c
cDC
Mφ
Mφ/Gra
CD11b
NK1.1
NK
NKT
CD3
CD8α
CD8
CD4
γδ+T
TCRγδ
Aii
Cell Number (x10⁵)
PBS
Cerulein
CD11b high CD11c -
CD11b high CD11c high-low
CD11b low CD11c high
NK
NKT
CD4+ T
CD8+ T
γδ+T
Bi
PBS
Cerulein
S1
S2
S3
Gr-1
Ly6G
Ly6C
Bii
S1
S2
S3
n.s.
Cell Number (x10⁵)
PBS Cerulein
C
10μm
Ly6C high
Ly6C low
D
CD3
NK1.1
Dx5
B220
F4/80
CD11c
Ly6C
Ly6G
CD80
CD86
PBS
Cerulein
S1
S2
S3
E
MFI
PBS
Cerulein
S1 S2 S3
CD80
CD86

neally at intervals of 1 hour (total of 8 injections). Mice were euthanized by cervical dislocation at 1 hour after the last cerulein injection. For L-arginine (L-Arg)–induced acute pancreatitis, L-Arg monohydrochloride (Sigma-Aldrich) was dissolved in saline and administered intraperitoneally in 2 dosages of 4 g/kg spaced 1 hour apart and mice were euthanized 72 hours later.

Statistical Analysis

Mann–Whitney *U* test was used for statistical analysis of the histological scores, and an unpaired Student *t* test was used for other analyses. All statistical analyses were performed with JMP software version 7.0 (SAS Institute Inc., Cary, NC), and values of $P < .05$ were considered to indicate statistical significance. All graphs were drawn using GraphPad Prism 5 for Windows (GraphPad Software Inc., San Diego, CA), and all data are presented as mean ± standard error of mean.

Results

Lymphocyte-Deficient Mice Develop Less Severe Cerulein-Induced Pancreatitis

Although accumulating evidence suggests a critical involvement of immune compartments in the pathogenesis of acute pancreatitis,[11–13] the mechanisms of their migration and activation for development of the disease remain unknown. To clarify these mechanisms, we used a murine model of acute pancreatitis induced by cerulein administration.[13,16] A landmark article by Demols et al[13] emphasized the importance of $CD4^+$ T cells by showing that the disease severity in T-cell–lacking *nu/nu* mice injected with cerulein is significantly decreased compared with that in wild-type (WT) mice in this model. We confirmed that cerulein-injected recombinase-activated gene-2 $(RAG2)^{-/-}$ mice, which lack both T and B cells, developed less severe pancreatitis than similarly treated WT mice (Supplementary Figure 1*A–C*). Notably, however, the serum levels of amylase and lipase in cerulein-administered RAG-$2^{-/-}$ mice were significantly higher than those in PBS-treated RAG-$2^{-/-}$ mice (Supplementary Figure 1C).

To investigate the roles of immune cells in this model, we used various gene-knockout mice and mice treated with an anti-asialo GM1 monoclonal antibody (Supplementary Figure 2). However, all the mice injected with cerulein developed comparable levels of pancreatitis to paired littermate controls based on the levels of serum amylase (Supplementary Figure 2), suggesting that the presence of lymph nodes and Th17, T-cell receptor (TCR)$\gamma\delta^+$, natural killer (NK), and natural killer T (NKT) cells play no positive pathological roles in this model. Based on these investigations, we hypothesized that this model involves a much more innate immune system, and moved to further assess the role of antigen-presenting cells (APCs), especially macrophages.

$CD11b^{high}Gr\text{-}1^{low}$ and $CD11b^{high}Gr\text{-}1^{high}$ Subpopulations Are Markedly Increased in the Pancreas of Cerulein-Injected Mice

To segmentalize the APC compartments in the pancreas, we stained pancreatic cells obtained from WT mice administered PBS or cerulein with paired monoclonal antibodies against CD11b/CD11c, CD3/NK1.1, CD4/CD8α, or CD3/TCR$\gamma\delta$. Three representative APC compartments were found in the PBS-administered pancreas: $CD11b^{low}CD11c^{high}$ classical dendritic cells (cDCs), $CD11b^{high}CD11c^{low\text{-}high}$ macrophages, and a small population of $CD11b^{high}CD11c^-$ macrophages/granulocytes (Figure 1*Ai*). Surprisingly, however, the ratio and absolute cell number of the $CD11b^{high}CD11c^-$ population were markedly increased in the pancreas of cerulein-injected mice (PBS, $0.34 \pm 0.03 \times 10^5$ vs cerulein, $12.66 \pm 4.86 \times 10^5$; $P = .019$) (Figure 1*Ai* and *Aii*). The other compartments of APCs in the pancreas of cerulein-injected mice were comparable with those in PBS-administered mice (Figure 1*Ai* and *Aii*). Ratios and absolute cell numbers of other immune compartments, such as $CD4^+$ and $CD8^+$ T, NKT, NK, and TCR$\gamma\delta^+$ T cells, were similar in PBS- and cerulein-administered mice (Figure 1*Ai* and *Aii*).

To separate the emerged $CD11b^{high}CD11c^-$ population in the pancreas after cerulein administration, we stained these cells with monoclonal antibodies against the paired CD11b and Gr-1 (Figure 1*Bi, upper panel*).[17] The major subpopulation of $CD11b^{high}$ cells before cerulein administration was the $CD11b^{high}Gr\text{-}1^-$ subpopulation (hereafter designated S1, *purple*). Although the ratio and absolute cell number of the S1 subpopulation in mice administered cerulein were comparable in the 2 groups, the ratios and absolute cell numbers of both the $CD11b^{high}Gr\text{-}1^{low}$ (S2, *green*) and $CD11b^{high}Gr\text{-}1^{high}$ (S3, *blue*) subpopulations were significantly higher than those in PBS-admin-

Figure 1. Cerulein administration induces marked infiltration of $CD11b^{high}Gr\text{-}1^{low/high}$ cells in the pancreas of cerulein-induced pancreatitis. (*Ai*) Expression of CD11b/CD11c, CD3ε/NK1.1, CD4/CD8α, and CD3ε/TCR$\gamma\delta$ on cells isolated from the pancreas of cerulein-injected (*Cerulein*) and PBS-injected (*PBS*) mice. The *boxes* indicate: cDCs, $CD11b^{low}CD11c^{high}$; macrophages, $CD11b^{high}CD11c^{low\text{-}high}$; macrophages/granulocytes, $CD11b^{high}CD11c^-$; NK cells, $CD3^-NK1.1^{high}$; NKT cells, $CD3^+NK1.1^{low}$; $CD4^+$ cells, $CD4^+CD8^-$; $CD8^+$ cells, $CD4^-CD8^+$; and TCR$\gamma\delta^+$ cells, $CD3^+$TCR$\gamma\delta^+$ cells. Data are representative of 3 independent experiments (5 mice/group). (*Aii*) Absolute cell numbers of each compartment in the pancreas of PBS-injected (*white*) and cerulein-injected (*red*) mice. Data are mean ± standard error of mean (SEM) (n = 7/group). *$P < 0.05$. *Mφ*, macrophages; *cDC*, classical DCs; *Gra*, granulocytes. (*Bi*) Expression of CD11b/Gr-1 (*upper*) and Ly6C/Ly6G (*lower*) on cells isolated from the pancreas of cerulein-injected (*right, Cerulein*) and PBS-injected (*left, PBS*) mice. The *boxes* indicate: S1, $CD11b^{high}Gr\text{-}1^-$; S2, $CD11b^{high}Gr\text{-}1^{low}$; and S3, $CD11b^{high}Gr\text{-}1^{high}$. Cells in the S1 (*purple*), S2 (*green*), and S3 (*blue*) subpopulations correspond to the indicated *dots of the same color* according to the FACSDiva analysis. (*Bii*) Absolute cell numbers of the three subpopulations in the pancreas of PBS- or cerulein-administered mice. Data are mean ± SEM (n = 7/group). *$P < .05$. (*C*) Morphologies of Giemsa-stained cells in the S1, S2, and S3 subpopulations. Data are representative of 2 independent experiments. (*D*) Surface expression of various molecules on the 3 subpopulations. Data are representative of 5 independent experiments. (*E*) Mean fluorescent intensities of CD80 and CD86 on the 3 subpopulations. Data are mean ± SEM (n = 4/group). *$P < .05$. MFI, mean fluorescent intensity; n.s., not significant.

istered mice (Figure 1*Bii*). Furthermore, S2 cells highly expressed Ly6C, but not Ly6G, and S3 cells highly expressed Ly6G, but with dominant Ly6C^{low} or minor Ly6C^{high} expression (Figure 1*Bi, lower panel*). Furthermore, morphologic analyses of sorted cells showed that the S1 and S2 subpopulations were macrophage-like, while the S3 subpopulation was a mixture of granulocyte-like cells with segmented nuclei (Ly6C^{low}) and macrophage-like cells with horseshoe-shaped nuclei (Ly6C^{high}) (Figure 1*C*).

Next, we evaluated the phenotypes of the pancreatic S1, S2, and S3 cells by staining with a third monoclonal antibody. None of the 3 subpopulations from PBS- or cerulein-injected mice expressed CD3, NK1.1, DX5, or B220 (Figure 1*D*). Irrespective of whether PBS or cerulein was injected, S1 and S2 cells expressed F4/80, and S3 cells did not, indicating that S3 cells were nonmacrophages composed of segmented granulocytes (Ly6C^{low}) and macrophage-like myeloid-derived suppressor cells (MDSCs) (Ly6C^{high}).[18] In addition, S1, but not S2, cells expressed CD11c. Thus, S1, S2, and S3 cells represented CD11c^{+} macrophages, CD11c^{-} macrophages, and granulocytes/MDSCs, respectively. Before the injection, Ly6C was not expressed on S1 cells, but was expressed on S2 cells at high levels and on S3 cells at moderate levels. After the injection, a substantial proportion of S1 cells showed up-regulated Ly6C expression, and S2 cells maintained high levels of expression. Interestingly, almost all the S3 cells maintained moderate expression levels of Ly6C, while a small but substantial proportion of these cells expressed Ly6C at high levels. In contrast, Ly6G was preferentially expressed on S3 cells (Figure 1*D*). Although all 3 fractions expressed CD80 and CD86 at low levels in PBS-injected mice, these levels were significantly increased in cerulein-injected mice (Figure 1*E*).

CCR2/CCL2-Dependent Migration of Inflammatory Macrophages Is Involved in Cerulein-Induced Pancreatitis

Given the findings that both S2 and S3 cells were markedly increased in the pancreas of cerulein-injected mice, we attempted to determine whether these subpopulations were pathogenic or protective in the process of pancreatitis development using CCL2 (macrophage chemoattractant protein-1)$^{-/-}$ mice, because CCL2 is a representative chemokine for the migration of monocytes/macrophages, but not granulocytes.[19] Although 2 previous reports showed amelioration of the disease by administration of a plasmid vector containing a dominant-negative mutant CCL2 gene in a rat cerulein-injection model[20] and a chemical blocker of CCL2 in a murine model,[21] these studies did not clarify the precise mechanisms of the effects in terms of the immune compartments. As expected, microscopic analyses revealed that the pathology in terms of the histological score was markedly milder in cerulein-administered CCL2$^{-/-}$ mice than in cerulein-administered WT mice (Figure 2*A* and *B*). Consistent with these findings, the serum amylase and lipase levels were significantly lower in cerulein-administered CCL2$^{-/-}$ mice than in cerulein-administered WT mice (Figure 2*C*). Notably, the ratio and absolute cell number of the S2 subpopulation, but not the S1 and S3 subpopulations, were significantly lower in cerulein-administered CCL2$^{-/-}$ mice than in cerulein-injected WT mice (Figure 2*D* and *E*), suggesting a pathological role of CD11b^{high} Gr-1^{low} S2 macrophages in this model. Interestingly, the expression levels of CD80 and CD86 on S1, S2, and S3 cells after cerulein injection were comparable in the 2 groups (Figure 2*F*), suggesting an independent mechanism for the activation of migrating cells in the pancreas.

Pathological Role of CD11b^{high}Gr-1^{low} Macrophages in Cerulein-Induced Pancreatitis

Next, we used mice depleted of monocytes/macrophages using clodronate before the cerulein challenge to assess the role of macrophages in this model. As expected, clodronate-administered mice developed less severe pancreatitis after cerulein injection compared with control mice based on the histology (Supplementary Figure 3*A*) and the serum levels of amylase and lipase (Supplementary Figure 3*B*), thereby confirming a pathological role of monocytes/macrophages in this cerulein-induced pancreatitis model. Interestingly, the clodronate protocol equally depleted approximately 80% of the S1, S2, and S3 subpopulations (Supplementary Figure 3*C* and *D*). Given the possibility that infiltrating macrophages are critically involved in the pathogenesis of this cerulein-induced pancreatitis model, we investigated whether infiltrating S2 or S3 cells induced pancreatic acinar cell apoptosis in vitro. We found that in vitro cultures with cerulein showed significantly increased ratios of apoptotic acinar cells compared with in vitro cultures without cerulein, and also found that addition of S2, but not S3, cells further increased the ratios of apoptotic cells, irrespective of the numbers of total (Annexin V [AV]$^{+}$ 7-amino actinomycin D$^{+/-}$), early (AV^{+}7-amino actinomycin D–), or late (AV^{+}7-amino actinomycin D^{+}) apoptotic cells. Notably, all S2 cell-induced apoptosis was abolished by the addition of neutralizing anti-tumor necrosis factor-α (TNF-α) monoclonal antibodies (Supplementary Figure 4).

Hemodynamics of Macrophages and Granulocytes in the Pathogenesis of Cerulein-Induced Pancreatitis

To further determine the hemodynamics of the increased numbers of S2 macrophages and S3 granulocytes/MDSCs in this model, we conducted parabiosis surgery between Ly5.1- and Ly5.2-background WT mice. At 2 weeks after the parabiosis surgery, we administered cerulein or PBS by intraperitoneal injection to the parabionts (Figure 3*A*). Before the injection, we confirmed that the proportions of S1 and S2 macrophages in the pancreas were significantly lower than those in the spleen, whereas those of S3 cells were comparable in the pancreas and spleen (Supplementary Figure 5). As expected, neither mouse in group 1 showed any inflammatory changes in